Methane sources, distributions, and fluxes from cold vent sites at Hydrate Ridge, Cascadia Margin

Katja U. Heeschen,[1,2,3] Robert W. Collier,[1] Marie A. de Angelis,[4] Erwin Suess,[5] Gregor Rehder,[5] Peter Linke,[5] and Gary P. Klinkhammer[1]

Received 24 March 2004; revised 24 September 2004; accepted 11 February 2005; published 5 May 2005.

[1] To constrain the fluxes of methane (CH_4) in the water column above the accretionary wedge along the Cascadia continental margin, we measured methane and its stable carbon isotope signature ($\delta^{13}C$-CH_4). The studies focused on Hydrate Ridge (HR), where venting occurs in the presence of gas-hydrate-bearing sediments. The vent CH_4 has a light $\delta^{13}C$-CH_4 biogenic signature (−63 to −66‰ PDB) and forms thin zones of elevated methane concentrations several tens of meters above the ocean floor in the overlying water column. These concentrations, ranging up to 4400 nmol L^{-1}, vary by 3 orders of magnitude over periods of only a few hours. The poleward undercurrent of the California Current system rapidly dilutes the vent methane and distributes it widely within the gas hydrate stability zone (GHSZ). Above 480 m water depth, the methane budget is dominated by isotopically heavier CH_4 from the shelf and upper slope, where mixtures of various local biogenic and thermogenic methane sources were detected (−56 to −28‰ PDB). The distribution of dissolved methane in the working area can be represented by mixtures of methane from the two primary source regions with an isotopically heavy background component (−25 to −6‰ PDB). Methane oxidation rates of 0.09 to 4.1% per day are small in comparison to the timescales of advection. This highly variable physical regime precludes a simple characterization and tracing of ''downcurrent'' plumes. However, methane inventories and current measurements suggest a methane flux of approximately 3×10^4 mol h^{-1} for the working area (1230 km^2), and this is dominated by the shallower sources. We estimate that the combined vent sites on HR produce 0.6×10^4 mol h^{-1}, and this is primarily released in the gas phase rather than dissolved within fluid seeps. There is no evidence that significant amounts of this methane are released to the atmosphere locally.

Citation: Heeschen, K. U., R. W. Collier, M. A. de Angelis, E. Suess, G. Rehder, P. Linke, and G. P. Klinkhammer (2005), Methane sources, distributions, and fluxes from cold vent sites at Hydrate Ridge, Cascadia Margin, *Global Biogeochem. Cycles*, *19*, GB2016, doi:10.1029/2004GB002266.

1. Introduction

[2] Atmospheric methane (CH_4) is a greenhouse gas that absorbs infrared radiation 25 times more efficiently than CO_2 [*Lelieveld et al.*, 1993, 1998]. There has been a renewed effort to study the possible sources of CH_4 entering the atmosphere because of the potential importance of CH_4 in climate changes in the past [e.g., *Dickens et al.*, 1995; *Kennett et al.*, 2000, 2003; *Hesselbo et al.*, 2000; *Kennedy et al.*, 2001; *Kasting and Siefert*, 2002] and because there has been a continuous increase in its atmospheric concentration over the past 150 years [*Etheridge et al.*, 1992; *Lelieveld et al.*, 1998]. A substantial ''unknown'' in the global methane budget is the nature and fate of CH_4 in the oceans and, in particular, along the continental margins, such as the Cascadia Margin. In these environments, methane clathrate hydrates can be significant reservoirs. The stability zone for these hydrates, which depends on conditions of temperature and pressure, usually begins at water depths below 300–500 m [*Kvenvolden*, 1993]. The estimates of the amount of methane stored in gas hydrates worldwide range between 1×10^{15} and 115×10^{15} m^3 of methane at STP, constituting by far the largest reservoir of CH_4 known [*Kvenvolden*, 1988, 1993, 1999; *MacDonald*, 1990; *Gornitz and Fung*, 1994; *Milkov*, 2004]. These reservoirs may have an important impact on the global carbon cycle [*Kvenvolden*, 2002; *Dickens*, 2003].

[1]College of Oceanographic and Atmospheric Sciences, Oregon State University, Corvallis, Oregon, USA.
[2]Also at GEOMAR Research Center for Marine Geology, Kiel, Germany.
[3]Now at Research Center Ocean Margins, University of Bremen, Bremen, Germany.
[4]Oceanography Department, Humboldt State University, Arcata, California, USA.
[5]Leibniz Institute of Marine Sciences, IFM-GEOMAR, Kiel, Germany.

0886-6236/05/2004GB002266$12.00

[3] Until recently, the ocean was thought to play a minor role in the present-day atmospheric CH_4 budget, accounting for just 2–4% (10–20 Tg CH_4 yr^{-1}) of the total methane released to the atmosphere [*Cicerone and Oremland*, 1988; *Bates et al.*, 1996]. Since the discovery of new shelf vent sites and "cold vents" related to sedimentary gas hydrates, estimates of the CH_4 emission rate to the atmosphere from the seabed have been revised and range from 18–48 Tg CH_4 yr^{-1}, or 4–9% of the global budget [*Hornafius et al.*, 1999; *Judd*, 2000; *Judd et al.*, 2002; *Kvenvolden et al.*, 2001]. An equivalent amount of seabed methane is thought to dissolve into seawater [*Kvenvolden et al.*, 2001]. A goal of ongoing research at continental margins is to obtain a better estimate of the impact of cold vents on the oceanic and atmospheric methane budget. In this paper, we describe data obtained from hydrate-bearing sites along the Oregon continental margin, and use these data to more accurately quantify the fate and flux of methane released from the seafloor.

[4] At the Cascadia subduction zone, where the Juan de Fuca Plate is subducted obliquely under the continental North American Plate, a thick accretionary complex has developed [*Kulm et al.*, 1986; *DeMets et al.*, 1990; *MacKay et al.*, 1992]. Our study focused on the characteristic morphological high within the secondary accretionary complex known as Hydrate Ridge (HR). As shown in Figure 1, Hydrate Ridge has two local topographic highs, the northern (NHR) and southern Hydrate Ridges (SHR). At NHR (depth = 590 m) the amplitude of tectonic folding is greatest, and it is characterized by extensive carbonate deposition at the surface [*Tréhu et al.*, 1999; *Johnson et al.*, 2000, 2003]. In contrast, SHR (depth = 790 m) has sediment layers that are tightly folded, and it is predominantly covered with more recent sediments. Two additional ridges of the secondary accretionary complex are South-East Knoll (SE-Knoll; depth = 620 m), which resembles NHR, and North-West Knoll (NW-Knoll; depth = 900 m), which is sediment covered, similar to SHR [*Tréhu et al.*, 1999]. A strong, bottom-simulating reflector (BSR) under these ridges, at sub-bottom depths between 74 and 120 m, is evidence of extensive deposits of gas hydrates which are underlain by sediments containing free gas [*Tréhu et al.*, 1999, 2004; *Tréhu and Flueh*, 2001]. According to *MacKay et al.* [1994], the gas occupies 1–5% of the sediment porosity beneath the BSR at NHR. At SHR, shallow layers of gas hydrates even outcrop on the seafloor [*Suess et al.*, 1999, 2001].

[5] *Suess et al.* [1999] were the first to describe the importance of gas hydrates and free methane gas at Hydrate Ridge, where fault zones feed localized fluid and gas vents. The venting sites are surrounded by abundant chemoautotrophic communities which are supported by sulfate reduction and anaerobic oxidation of methane [*Boetius et al.*, 2000; *Elvert et al.*, 2000; *Sahling et al.*, 2002]. Thus much of the advecting methane is oxidized within the sediment and stored in either the chemosynthetic biomass or massive authigenic carbonates [*Bohrmann et al.*, 1998; *Greinert et al.*, 2001; *Teichert et al.*, 2003]. In the water column above the vent sites of NHR, *Suess et al.* [1999] found CH_4 concentrations to be 2 to 3 orders of magnitude above background levels. The heterogeneity of the CH_4 concentrations was thought to result from the spatial distribution of very active vent sources and their temporal fluctuations. Initial estimates of the dissolved methane flux into the water column ranged from 20 to 375 mol m^{-2} yr^{-1} [*Linke et al.*, 1994; *Suess et al.*, 1999; *Torres et al.*, 2002]. In contrast, very little is known about the fluxes of gaseous methane at these cold vent locations. Only the estimate of 22×10^6 mol yr^{-1} is known for a single vent site at NHR, where methane accounts for 99% of the vented gas phase [*Torres et al.*, 2002]. Modeling results [*Luff and Wallmann*, 2003] and water column measurements [*Grant and Whiticar*, 2002] demonstrate that the gas venting is an important process for transport of CH_4 into the water column at Hydrate Ridge. *Heeschen et al.* [2003] reported acoustic observations of methane gas plumes that consistently rose to just above the top of the gas hydrate stability zone (GHSZ; 510–490 m) at Hydrate Ridge and SE-Knoll.

[6] On the basis of these previous studies, the distribution of methane in the regional water column is mainly controlled by oxidation of methane derived from vent sources associated with gas hydrates [*Valentine et al.*, 2001; *Grant and Whiticar*, 2002]. However, the fluxes from other methane sources along the continental margin have not been characterized, and the complex hydrographic environment has not been considered. For example, Hydrate Ridge is located within the California Current system, the dynamic eastern boundary current of the NE Pacific, characterized by strong coastal upwelling due to the prevailing southerly winds during summer and early fall. This current system is characterized by extreme hydrographic variability, offshore transport in the surface Ekman layer, and the formation of a powerful, meandering, southward-flowing coastal jet with core velocities of 50 to 80 cm s^{-1} [*Huyer*, 1977, 1983; *Huyer et al.*, 1979, 1991; *Kosro and Huyer*, 1986]. The poleward-flowing geostrophic undercurrent with a core depth of 100–350 m has an average core layer velocity of 0.18 m s^{-1} and is found 20–25 km off the shelf break along the slope and can extend much deeper in the water column [*Huyer et al.*, 1991; *Kosro et al.*, 1991; *Pierce et al.*, 2000; *Kosro*, 2002]. The undercurrent frequently turns offshore and forms anticyclonic eddies, especially when passing coastal promontories [*Strub et al.*, 1991; *Collins et al.*, 1996; *Huyer et al.*, 1998; *Garfield et al.*, 1999; *Barth et al.*, 2000; *Pierce et al.*, 2000].

[7] The carbon isotopic composition of methane, $\delta^{13}C$-CH_4, has proven to be a particularly powerful tool for identifying different methane sources and tracing the flow of carbon through different reservoirs and processes such as oxidation or mixing [e.g., *Whiticar*, 1999]. Methane produced deep within the accretionary wedge by microbial activity (fermentation) is highly depleted in ^{13}C. This biogenic process results in isotopically light methane pools. The thermogenic production of CH_4 during thermal "maturation" of deeply buried sediments is not accompanied by significant isotopic fractionation and produces isotopically heavier methane that is closer in composition to its organic carbon source. According to *Whiticar* [1999], a diagnostic boundary between themogenic and biogenic CH_4 is found at roughly −50‰ PDB (Peedee Belemnite Standard). Extremely light carbon isotopic ratios of −71 to −62‰

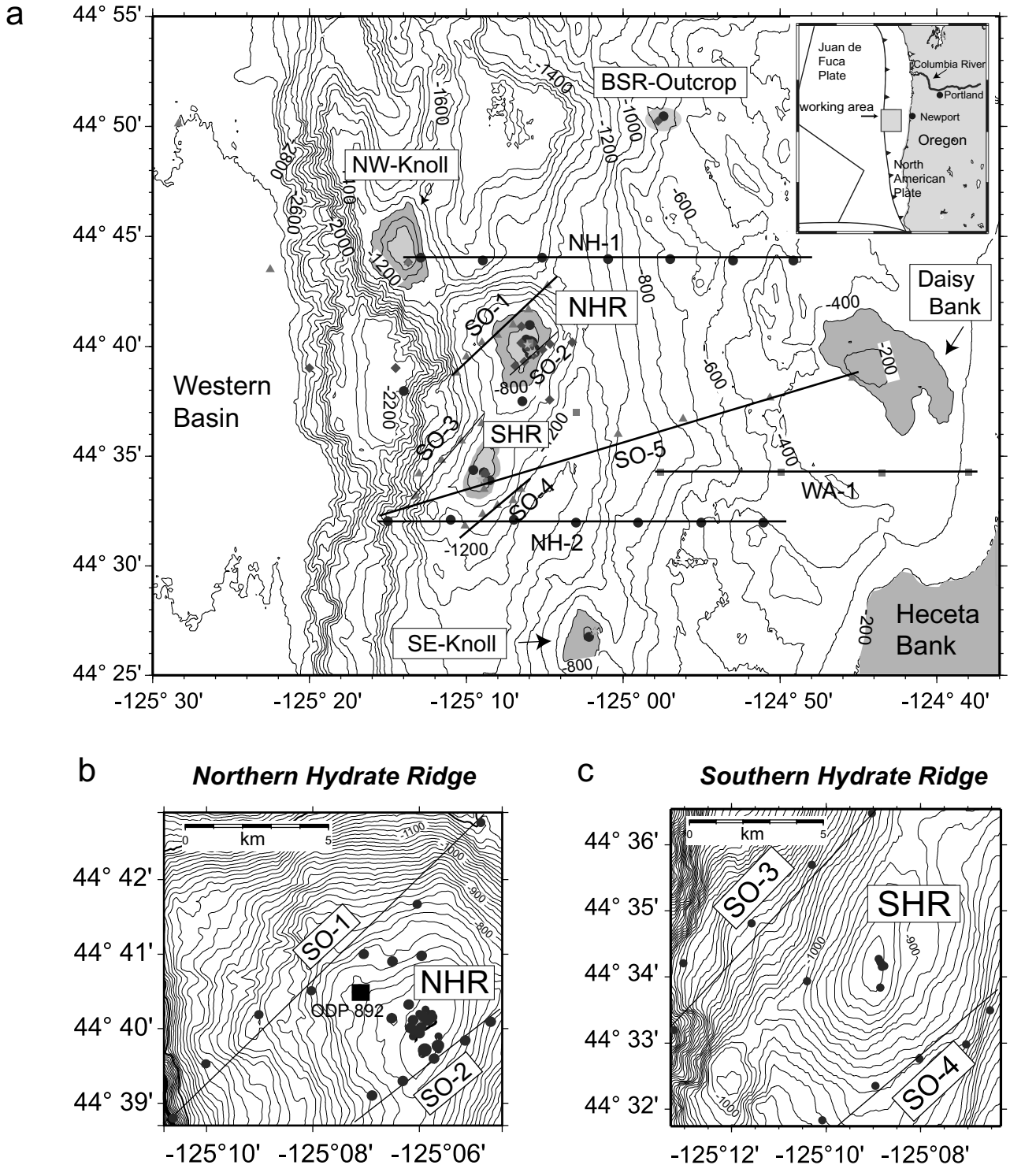

Figure 1. Sample locations and bathymetry of the TECFLUX study area. (a) Overview of the working area within the Cascadia Margin (inset) showing the locations of all CTD stations as well as the lines of the hydrographic sections shown in Figure 5. Enlarged views of (b) Northern Hydrate Ridge (NHR) and (c) Southern Hydrate Ridge (SHR) show the location of vent-focused and near-field sampling. For the location of Southern Temple, see Figure 10.

Table 1. TECFLUX Cruises With Water Column Program

Cruise	RV	Dates	Water Samples	Station Numbers	Objective
RB98-03-2A	*Ron Brown*	18 Aug. to 24 Aug. 1998	8 CTD casts	RB/1-20	preliminary investigation at NHR water column
NH0699	*New Horizon*	12 June to 22 June 1999	42 CTD casts	NH/1-53	search for sources at HR; large-scale sections for methane flux calculations; downstream casts
AT3-35b	*Atlantis*	30 June to 13 July 1999	6 CTD casts; sample bottles on Alvin	AT/1-37	continuing program from NH0699
SO143-1	*SONNE*	14 July to 30 July 1999	15 CTD casts; ZAPS tows	SO143/1-75	tide-dependent distribution in the source areas
SO143-2	*SONNE*	31 July to 25 Aug. 1999	23 CTD casts	SO143/75-199	time series at source area SHR; background CTD; tow-jo CTD at HR; section for flux calculations
W1099a	*Wecoma*	1 Oct. to 5 Oct. 1999	12 CTD casts; ZAPS tows	W/1-17	section from shelf - HR
SO148	*SONNE*	20 July to 15 Aug. 2000	25 CTD casts; sample bottles on ROPOS	SO148/1-106	sections for flux calculations; section shelf - HR

PDB are found in the gas hydrates at Hydrate Ridge and demonstrate its biogenic origin [*Kastner et al.*, 1998; *Suess et al.*, 1999]. On the other hand, there are natural gas vents found on the nearby shelf and slope off Oregon which have δ^{13}C-CH_4 values as heavy as −28‰ PDB, demonstrating a thermogenic origin [*Collier and Lilley*, 1995, 2005]. Microbial oxidation of methane results in a kinetic isotope fractionation due to the preferential use of ^{12}C over ^{13}C [*Whiticar*, 1999]. After significant oxidation of methane, this process results in residual methane pools that become isotopically heavier than the source methane.

[8] To help constrain the behavior and flux of methane in the water column which is associated with the significant reservoirs of methane hydrates and venting along continental margins, we acquired an extensive data set of methane concentrations and associated stable carbon isotope ratios between 1998 and 2000 along the Oregon Margin. The interpretation of these distributions required the simultaneous characterization of the Eastern Boundary current system including hydrographic properties and current observations.

2. Methods

[9] As listed in Table 1, the TECFLUX project comprised seven cruises over the Cascadia Margin off Oregon between 1998 and 2000, all of which included water column sampling [*Torres et al.*, 1998, 1999; *Bohrmann et al.*, 1999; *Linke et al.*, 2001]. During these cruises, samples for CH_4 concentrations and carbon isotopic compositions were collected from 130 vertical or towed CTD casts (Figure 1). Data from the 1998 cruise were discussed by *Suess et al.* [1999]. The complete data set from 1999 and 2000 is available in an auxiliary table[1].

[10] Seabird CTDs (conductivity, temperature, and depth sensors) and rosette samplers were used for hydrographic transects. All CTDs had been calibrated within 6 months of use. The CTDs were outfitted with oxygen sensors (SBE13) and optical turbidity sensors, including a transmissometer (SeaTech, 25 cm) and/or a backscatter sensor (SeaTech OBS). Additional water samples were collected from other vehicles including the ZAPS (towed Zero Angel Photometer System [*Klinkhammer and McManus*, 2001]), DSRV ALVIN, ROV ROPOS, and benthic landers.

[11] An in situ methane sensor (METS, GKSS-Forschungszentrum, Germany) was used during all CTD and ZAPS deployments. Although calibration was not generally possible for these dynamic systems because of the METS sensor's slow response time, it allowed qualitative observations and it was critical for positioning the sample collection and obtaining water samples from thin layers of CH_4-rich plumes [*Klinkhammer et al.*, 1999]. Hull-mounted echosounding systems with frequencies between 12–18 kHz were used to directly detect and track gas bubble plumes in the water column [*Heeschen et al.*, 2003].

[12] Two current meters (Alpha Omega, VACM 9605) were deployed on a mooring at 500 m and 600 m water depths. The mooring was located south of NHR (44°38.5′N, 125°06.4′W, bottom depth 673 m) and was deployed between April and October 1999.

[13] Oxygen concentrations were determined with the CTD oxygen sensor and confirmed by Winkler titration [*Grasshoff et al.*, 1983]. Methane concentrations in water samples were determined at sea using a modified vacuum degassing method [*Lammers and Suess*, 1994; *Rehder et al.*, 1999]. This entailed obtaining 400-mL samples of seawater from the rosette samplers using glass syringes and immediately transferring them into pre-evacuated 600-mL glass bottles. Head-space gas and water phases were allowed to equilibrate before the resulting gas phase was recompressed to atmospheric pressure, and the CH_4 mole fraction of the total extracted gas was determined by gas chromatography using flame ionization detection (FID). Bottled mixtures of 10.0 ppm ±2% and 1002 ppm ±5% CH_4 in synthetic air from Scotty Specialty Gases were used for standards. Replicate analyses of two series of samples from a single hydrocast with about 6 nmol L^{-1} (n = 9) and 0.16 nmol L^{-1} (n = 6) yielded a precision of 2% and 9%, respectively.

[1] Auxiliary material is available at ftp://ftp.agu.org/apend/gb/2004GB002266.

[14] The amount of dissolved CH_4 in each water sample was calculated as the product of the methane mole fraction in the extracted gas phase and the total amount of gas in the sample at STP. The total gas concentration of the sample was calculated by adding the measured dissolved oxygen concentration and the calculated nitrogen and argon concentrations. Nitrogen and argon concentrations were assumed to be at saturation relative to their atmospheric partial pressures, taking into account in situ temperatures and salinities [*Weiss*, 1970]. The degree of CH_4 saturation in the water relative to equilibrium with the atmosphere was determined with equations from *Wiesenburg and Guinasso* [1979] using an atmospheric CH_4 concentration of 1.79 ppm which was taken from the NOAA records (ftp://ftp.cmdl.noaa.gov/ccg/ch4/flask/month; cited September 2004). Because CH_4 has a solubility of about 2 mmol kg^{-1} seawater at 4°C and 1 atm [*Duan et al.*, 1992], it can be expected that no degassing occurred during sample recovery.

[15] The $\delta^{13}C$-CH_4 ratios in the gas extracted from the water samples were determined with a Continuous Flow Isotope Ratio Mass Spectrometer (CF-IRMS), applying a method originally described by *Merritt et al.* [1995] and modified by *Grant* [2000] at the SEOS laboratory of the University of Victoria. A Finnigan MAT 252 mass spectrometer (Finnigan, Bremen, Germany) was used in combination with a preparative sample pre-concentration loop and a gas chromatograph linked in series with a microvolume combustion reactor (Cu/CuO/Pt at 910°C). Following sample injection, the contaminants N_2 and O_2 were eluted from the gas samples in a cooled preparative column which contained a molecular sieve to retain CH_4. Water was removed using a selectively permeable Naphion® tubing assembly. To increase sensitivity, the open split was modified to maximize the amount of sample directed into the mass spectrometer. Replicate air samples with amplitudes as low as 300 mV yielded a precision of 0.8‰ PDB for samples measured in 1999 and 0.9‰ PDB for samples measured in 2000.

3. Results and Discussion

[16] To determine the behavior, significance, and associated flux of methane released from the cold vents of Hydrate Ridge and related features of the accretionary complex, we investigated the characteristics of the vent sources, the strong California Current, and the resulting distributions of methane and $\delta^{13}C$-CH_4 in the water column.

3.1. Methane Inputs and Distributions

3.1.1. Hydrate Ridge Vent Sites

[17] Dissolved methane in close proximity to the vent sites of southern and northern Hydrate Ridge (SHR and NHR) reaches extremely high concentrations and is very heterogeneous in time and space (Figures 2a–2c). The highest CH_4 concentrations were usually confined to thin layers, several tens of meters in thickness, and elevated 80 ± 50 m above the seafloor. Within these layers, CH_4 concentrations reached 1400 nmol L^{-1} at SHR and 4400 nmol L^{-1} at NHR. Methane maxima over 200 nmol L^{-1} were frequently accompanied by smaller separated peaks above and below (10–150 nmol L^{-1}). Between the peaks, concentrations often dropped to values less than 5 nmol L^{-1} and were sometimes as low as the regional background values of 0.5–1.5 nmol L^{-1}. At both NHR and SHR, the samples taken nearest to the bottom were usually elevated in CH_4, but only occasionally contained these most extreme concentrations.

[18] Methane concentrations in the water column near the vent sites also varied with time over 3 orders of magnitude (Figure 2c). Successive GPS-navigated CTD profiles from SHR and NHR, which are generally positioned to within a 50 m radius and taken over intervals of just a few hours, identify methane maxima that range between 10 nmol L^{-1} and 1000 nmol L^{-1}. Samples from a single CTD station, collected within a 1-hour period (on the downcast and upcast), showed concentration changes as large as 1 order of magnitude (Figure 2b: SO143/97-19).

[19] These highly variable and sharply-defined CH_4 maxima above the vent sites of SHR and NHR are likely caused by the transport and dissolution of methane bubbles from the seafloor as opposed to fluid-phase injection from the cold seeps. The highest concentrations of dissolved CH_4 detected by the METS sensor and rosette samples almost always occur when and where rising gas bubble plumes were detected by acoustic methods. Although mixed layers were frequently observed within 100 m above the HR vent sites (see section 3.3), the CH_4 peaks at these depths showed no correlation with density or other hydrographic structures which would be expected had the methane peaks been caused by the rise of methane-laden vent fluids. The cold vent fluids at Hydrate Ridge, with densities very similar to bottom water, spread outward along isopycnals, and are partly responsible for the elevated CH_4 concentrations seen in nearly all bottom samples. *Damm and Budéus* [2003] discuss a similar fate for dissolved methane from a cold seep in the Norwegian Sea, whereas patterns of trans-isopycnal methane distributions were found at the sites of natural gas vents such as at Coal Oil Point [*Clark et al.*, 2000] and in the gas-hydrate-bearing Eel River Basin [*Valentine et al.*, 2001].

[20] Ongoing research on dissolution processes within rising gas-bubble plumes at various hydrocarbon vent sites suggests that the bubbles can induce an upwelling flow (v_{up}) by transferring momentum to the surrounding fluids [*McDougall*, 1978; *Leifer et al.*, 2000; *Leifer and Judd*, 2002; *Leifer and Patro*, 2002]. As the bubbles rise in the water column, bubble size decreases (as long as the rate of dissolution overcomes the rate at which the bubble size increases owing to the hydrostatic pressure decrease). As bubble size decreases, v_{up} decreases to zero and the remaining gas phase is "deposited" in the water column at that depth. This process was termed "bubble deposition" by *Leifer and Judd* [2002]. The depth of maximum deposition strongly depends on the release radii of the bubbles, the seabed depth, the vertical velocity, and the hydrostatic pressure. Further, it will be altered by the gas-hydrate skin which armors the rising bubbles through the GHSZ and decreases the dissolution rate [*Rehder et al.*, 2002b]. *Heeschen et al.* [2003] observed that acoustic images of

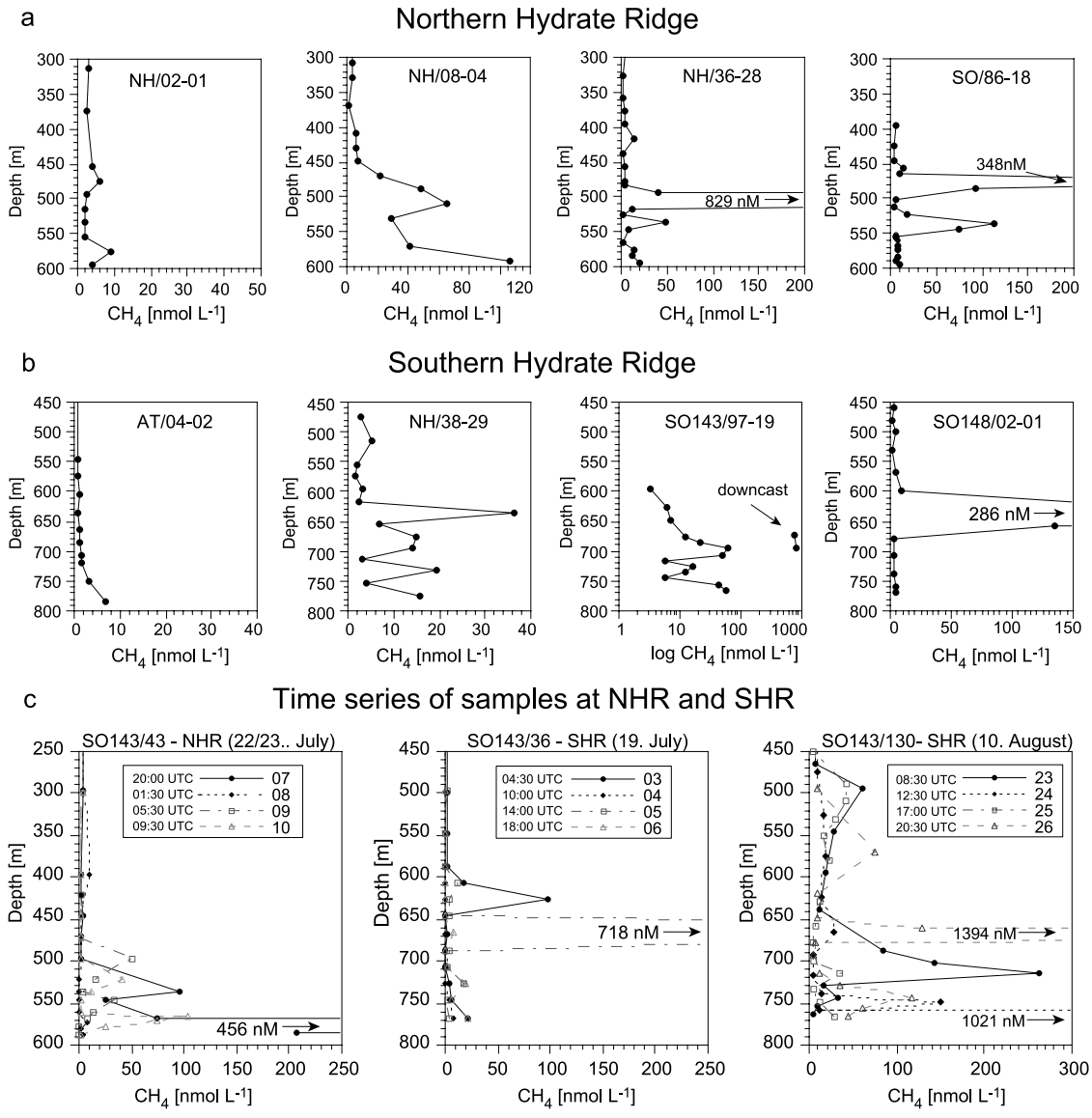

Figure 2. Examples of methane profiles in single CTD casts. Methane profiles for (a) NHR and (b) SHR. (c) Methane profiles for time series of samples at NHR and SHR. Note that different scales are used to display the methane concentrations in Figures 2a–2c, and that the depth scales differ as well.

bubble plumes at Hydrate Ridge vanished just above the GHSZ at water depths of 460 to 500 m. The depths of dissolved methane maxima above Hydrate Ridge, however, show that the maximum deposition depths are still within the GHSZ. The multiple peaks in methane concentration observed at Hydrate Ridge vent sites (Figure 2c) may relate to varying release radii or bubble plume input density. At NHR, there are at least three separate gas vents, further complicating the character of the vent plume.

[21] The variability of the gas venting activity at NHR has been well documented with video [*Torres et al.*, 2002; K. Nakamura, National Institute of Advanced Industrial Sciences and Technology, Japan, personal communication, 2002]. These observations demonstrate significant tidal components superimposed on gas venting activity at NHR. At SHR, where continuous video observations are lacking, our repeated hydrocasts suggest no tidal variations in the CH_4 concentrations (Figure 3). If all CH_4 maxima (>100 nmol L^{-1}) above NHR and SHR are compared to the tidal cycle, a correlation between low tide and highest CH_4 concentrations is found at NHR, but not at SHR. The contrasting behavior may relate to the different sub-bottom depths of the methane gas reservoirs, different sub-surface structures, or mechanisms triggering the gas venting. At NHR, deep faults reach below the relatively shallow BSR into areas of free methane gas [*MacKay et al.*, 1994; *Westbrook et al.*, 1994]. Changes in hydrostatic pressure with the tides may directly affect the movement and release of this gas. At SHR, the connection to the deeper BSR is more complex. Shallower faults, combined with a system of

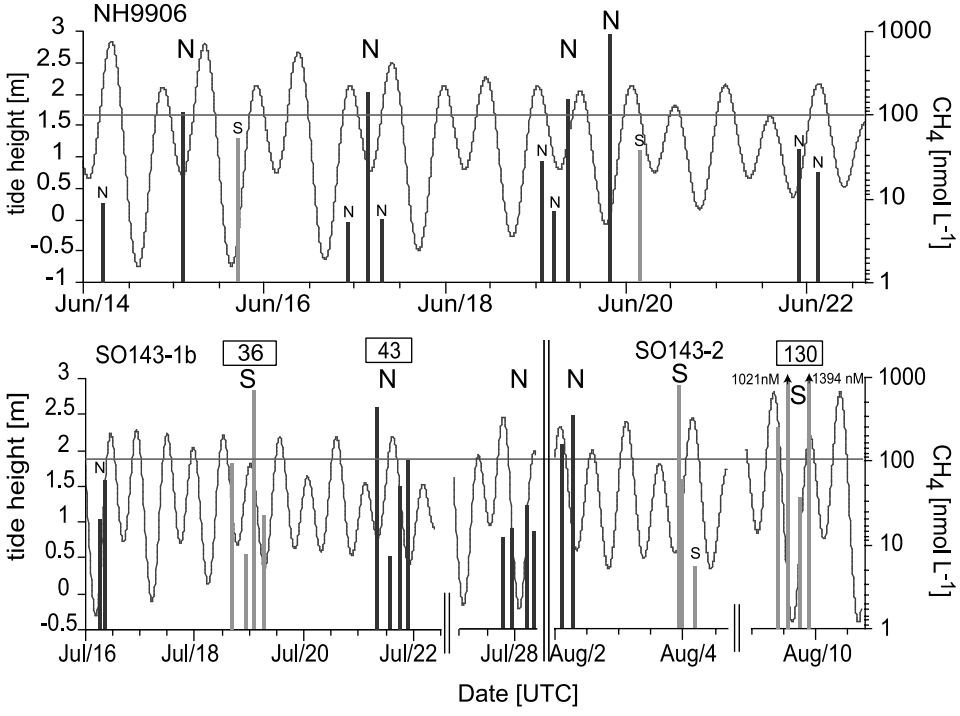

Figure 3. Correlation between the tidal cycle (at Newport harbor) and the methane maxima of each CTD cast at NHR (N, dark shading) and SHR (S, light shading) below 480 m depth over several weeks during summer 1999. For the correlation between methane ebullition and the tidal cycle, CH_4 maxima exceeding 100 nmol L^{-1} were taken into account. Low concentrations could either result from a shut down of the source or be a sampling artifact caused by changing current directions. The station numbers of the time series shown in Figure 2c are marked in the boxes above the lower diagram.

lithologically-controlled permeability variations in the sediment, were recently described as possible fluid and gas pathways at SHR [*Tréhu et al.*, 2004]. Gas hydrate dynamics or changes in gas pressure might control the gas release [*Suess et al.*, 1999; *Tryon et al.*, 1999].

3.1.2. Other Submarine Features of the Accretionary Complex

[22] In addition to the data from HR, hydrographic studies were undertaken at four other distinct submarine features: SE-Knoll, NW-Knoll, the BSR-Outcrop to the north at 500 m depth [*Tréhu et al.*, 1995], and a mound-like structure to the south, called "Southern Temple" (Figures 1 and 10). All of these features proved to be active methane sources (Figure 4). The CH_4 profiles near the summit of SE-Knoll resemble those of the Hydrate Ridge vent sites and suggest active methane gas venting. However, CH_4 maxima observed at SE-Knoll were 2 orders of magnitude lower than at HR. The profiles above NW-Knoll and the BSR outcrop had maximum CH_4 concentrations in the samples closest to the seafloor (11 nmol L^{-1}). These were probably caused by

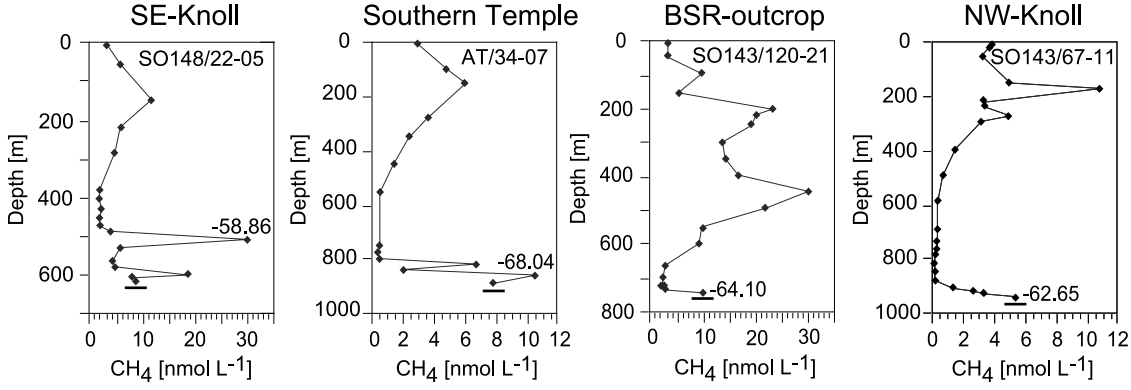

Figure 4. Methane profiles and the stable carbon isotopic signatures (‰ PDB) of deep methane maxima obtained from other submarine features.

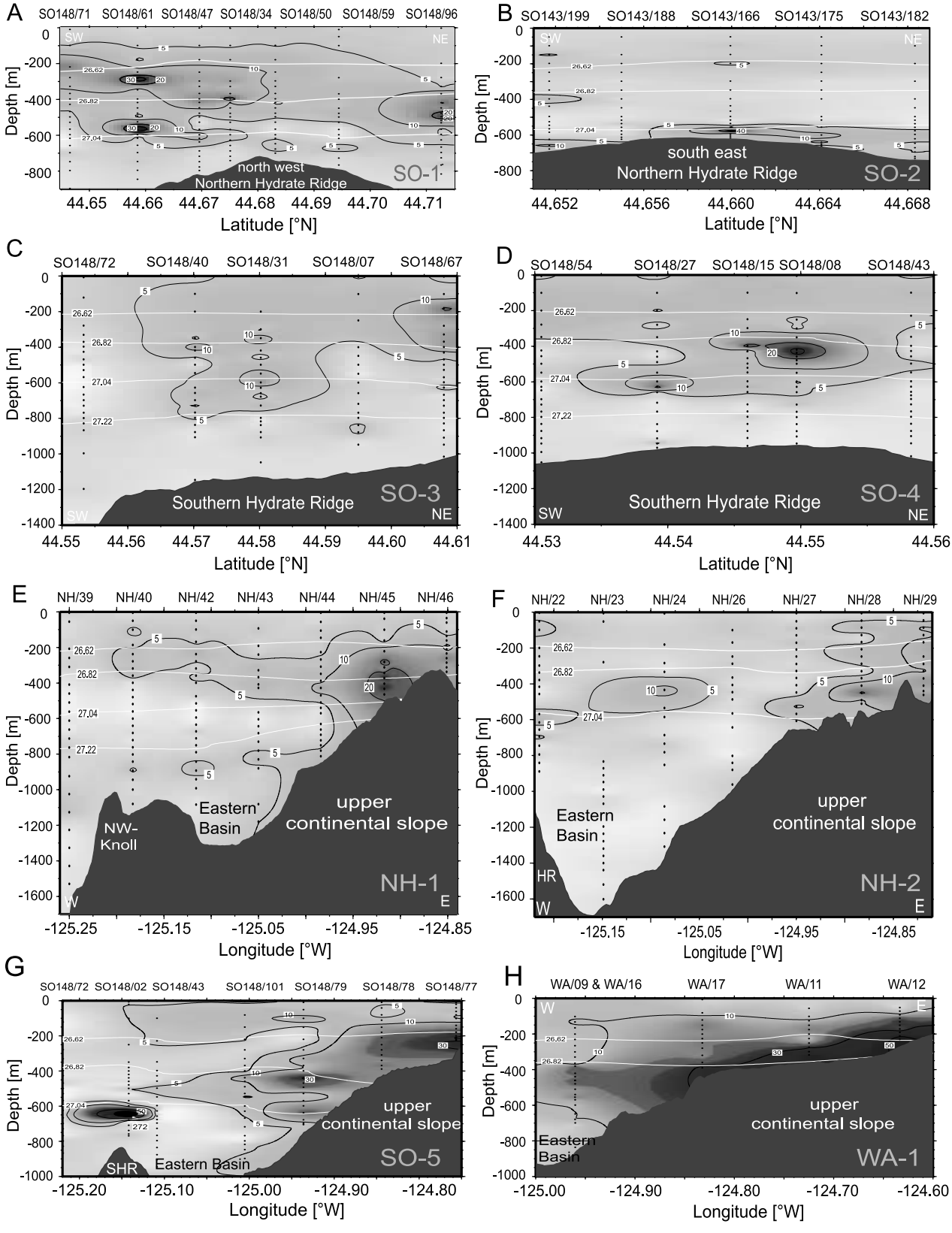
A
SO148/71 SO148/61 SO148/47 SO148/34 SO148/50 SO148/59 SO148/96
SW
NE
north west
Northern Hydrate Ridge
SO-1
Depth [m]
Latitude [°N]
B
SO143/199 SO143/188 SO143/166 SO143/175 SO143/182
south east
Northern Hydrate Ridge
SO-2
C
SO148/72 SO148/40 SO148/31 SO148/07 SO148/67
Southern Hydrate Ridge
SO-3
D
SO148/54 SO148/27 SO148/15 SO148/08 SO148/43
Southern Hydrate Ridge
SO-4
E
NH/39 NH/40 NH/42 NH/43 NH/44 NH/45 NH/46
NW-
Knoll
Eastern
Basin
upper
continental slope
NH-1
Longitude [°W]
F
NH/22 NH/23 NH/24 NH/26 NH/27 NH/28 NH/29
Eastern
Basin
upper
continental slope
HR
NH-2
G
SO148/72 SO148/02 SO148/43 SO148/101 SO148/79 SO148/78 SO148/77
upper
continental slope
SHR
Eastern Basin
SO-5
H
WA/09 & WA/16 WA/17 WA/11 WA/12
upper
continental slope
Eastern
Basin
WA-1
0 2 5 10 15 20 25 30 35 40 45 60
CH4 [nmol/L]

Figure 5

venting of methane-laden fluids. At Southern Temple, elevated CH_4 concentrations (up to 12 nmol L^{-1}) were spread over 80 m of the water column above the mound, suggesting a weak bubble ebullition or strong fluid flow and enhanced vertical mixing, which is common in this area.

3.1.3. Regional Methane Distribution

[23] The cold-seep sources discussed above introduce methane into the complex California Current environment. The variable current regime coupled with the temporal variability of the venting prevents the formation of downcurrent CH_4 plumes. Instead, methane is more widely dispersed and its distribution is further altered by offshore transport from shelf and upper slope sources (Figure 5). In order to better constrain these methane inputs over larger spatial scales, a series of hydrographic sections was collected across the Cascadia Margin. These sections were located in an attempt to constrain the fluxes from NHR (SO-1 and -2) and SHR (SO-3 and -4) as well as the full margin section and shelf/slope sources (NH-1, NH-2, SO-5, WA-1) (Figure 1).

[24] The CH_4 concentrations in the water column rapidly decline with lateral distance from the vent sites at NHR and SHR (Figure 5). At distances of 1–3 km from these vents, maximum CH_4 concentrations did not exceed 40 nmol L^{-1} and were not preferentially higher in any direction away from the vents (Figures 5a–5d). In hydrographic sections obtained further north (NH-1) and south (NH-2) of HR (Figures 5e and 5f), CH_4 concentrations were already less than 8 nmol L^{-1}.

[25] In comparison with the deep water CH_4 enrichments at Hydrate Ridge, offshore methane maxima above 480 m depth were usually broader, reaching concentrations as high as 35 nmol L^{-1} (Figures 5a–5h). Throughout the working area the water column was usually elevated in methane between 100 to 300 m depth. The measured concentrations of 5 to 22 nmol L^{-1} CH_4 corresponded to 100–600% supersaturation with respect to the recent atmospheric mole fraction of CH_4 of 1.79 ppmV. The hydrographic sections on this continental margin clearly show strong sources of methane at the shelf edge seafloor (Figures 5e–5h). Also, in situ production of methane is common in the upper water column [*Karl and Tilbrook*, 1994]. Near-bottom samples taken from just off the shelf had maximum CH_4 concentrations of 55 nmol L^{-1} (Figure 5h). There was a higher frequency of maxima above 480 m in sections collected in the year 2000 (SO-1,-3,-4,-5) compared to those collected in 1999 (SO-2, NH-1, NH-2, WA-1).

[26] In surface water the process of air-sea exchange causes smaller CH_4 supersaturations. They 34% in 1999 and 65% in 2000. These values are similar to continuously measured surface methane concentrations obtained in 1999 by *Rehder et al.* [2002a], who found only small supersaturations in the area of Hydrate Ridge, while toward the shelf edge, the saturation increased to 150% owing to coastal upwelling.

3.2. Methane Sources and Biogeochemical Processes

[27] Figure 6a illustrates the depth distribution of the stable carbon isotope ratios of methane, $\delta^{13}C\text{-}CH_4$, in water samples collected at Hydrate Ridge vent sites. It shows that the isotope signatures are clearly separated into two groups, a shallow group with relatively heavy $\delta^{13}C\text{-}CH_4$ signatures and a deep group with much lighter ratios. At both NHR and SHR, the shallow water samples have values between −12 and −40‰ PDB, whereas below 480 m water depth, the $\delta^{13}C\text{-}CH_4$ signatures ranged between −42 and −68‰ PDB. The delineation between the two groups is very sharp and occurs at the same depth for both NHR and SHR, despite the different bottom depths of the vents. The depth of change in $\delta^{13}C\text{-}CH_4$ is consistent with the upper limit of the GHSZ at 490–510 m, the upper limit of the weakening bubble plumes, and at the same time marks a discontinuity in the hydrographic regime, the details of which are discussed below. These results indicate that the methane budgets below and above 480 m are dominated by different methane sources.

[28] The origin of the two methane isotopic groups can be interpreted from the $\delta^{13}C\text{-}CH_4$ as a function of CH_4 concentrations for all samples analyzed in the working area (Figure 6b). This correlation shows two distinct peaks, one between −28 and −38‰ PDB and the other between −58 and −68‰ PDB. These peaks represent the isotopic endmembers of the two main methane sources contributing to the inventory.

[29] The isotopically light end-member measured in water samples within the GHSZ above HR is very well defined, and according to the classification of *Whiticar* [1999] the methane is of biogenic origin. The highest CH_4 concentrations at HR have $\delta^{13}C\text{-}CH_4$ values that are identical to those measured in vent gas taken with the submersible *Alvin*. The average $\delta^{13}C\text{-}CH_4$ value of the gas was −66‰ PDB at SHR and −63‰ PDB at NHR. Differences in gas pathways, storage, or gas hydrate formation may lead to differences in the availability for microbial oxidation.

[30] At 400 m, very few elevated methane concentrations with light $\delta^{13}C\text{-}CH_4$ signatures suggested scarce transport of NHR vent gas above the GHSZ (Figure 6a). At this depth, isotopically heavier methane accounts for nearly the entire methane inventory. This end-member with intermediate concentrations has a wider range of isotopic ratios and relates to sources on the shelf and upper slope. It is observed in near-bottom water samples close to the shelf edge and in the numerous CH_4 peaks at depths of about 400 m and shallower. The $\delta^{13}C\text{-}CH_4$ signatures measured in waters above the upper continental slope (Figure 6b, triangles)

Figure 5. Methane concentrations along regional transects shown in Figure 1. (a, b) SO-1 and SO-2, showing cross sections from NE-SW transects in the area of NHR; (c, d) SO-3 and SO-4, showing cross sections from NE-SW near SHR. (e, f, g) NH-1, NH-2, and SO-5, showing cross sections from the upper continental slope to the HR areas; (h) WA-1, showing a cross section of the upper slope only. Note that there is considerable variation in the latitudinal and longitudinal scales of the figures. The black dots indicate all samples taken, and station numbers are annotated in the top of each figure. The density distribution is shown by the annotated white (red) contours. See color version of this figure at back of this issue.

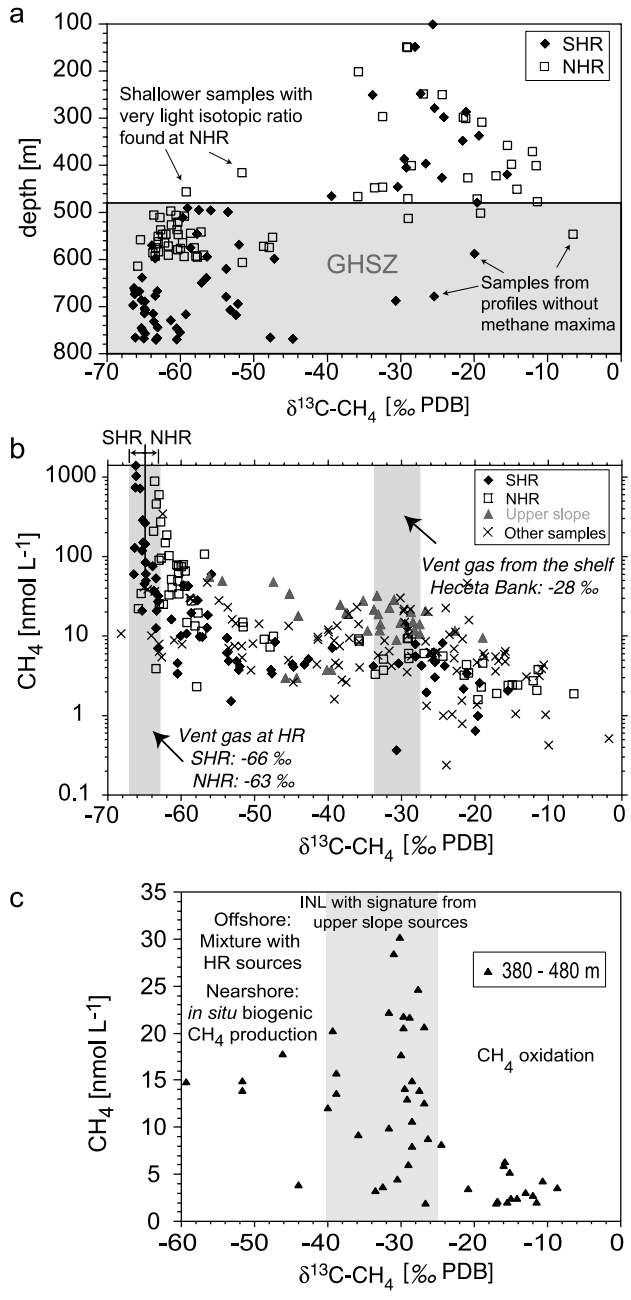

Figure 6. (a) Plots of depth versus carbon isotopic ratios of methane in the vicinity of NHR and SHR vent sites. There is a sharp shift in the carbon isotope ratios of methane at 480 m depth. The upper limit of the gas hydrate stability zone (shading) at HR is derived from an equation of *Dickens and Quinby-Hunt* [1994] for pure methane gas using the temperature profiles taken at HR during the TECFLUX investigations. (b) Plots of methane concentrations versus carbon isotopic ratios of methane. The shaded areas mark the range of carbon isotopic ratios found in methane gas at Hydrate Ridge (HR) and vent gas on the shelf, respectively [*Collier and Lilley*, 1995]. (c) Plots of methane concentrations versus carbon isotopic ratios of methane from all water samples in the depth range of 380–480 m. They resemble δ^{13}C-CH_4 ratios form Heceta Bank vent sites and upper slope water samples.

varied between −20 and −56‰ PDB, suggesting that this methane originates from a variety of sources. In section NH-1 (Figures 1 and 5a), the δ^{13}C-CH_4 signature below the shelf edge (460 m water depth) is −28‰ PDB (15 nmol L^{-1}). According to the classification of *Whiticar* [1999], this signature indicates methane of thermogenic origin. In contrast, near-bottom water samples from 230 m depth in section WA-1 (Figures 1 and 5h) have a light δ^{13}C-CH_4 signature of −56‰ PDB (55.2 nmol L^{-1}), probably resulting from seepage of biogenic methane produced in the sediments by microbial methanogenesis. Mixed intermediate ratios of −40‰ PDB are found in near-bottom water samples at depths of 400 to 600 m at the slope in SO-5 (Figures 1 and 5g).

[31] The majority of CH_4 concentration maxima sampled between 350 to 450 m depths throughout the working area have isotopic ratios between −26 to −34‰ PDB (Figure 6c). Samples obtained from CH_4 maxima above 350 m have similar isotope ratios (−25 to −35‰ PDB). These heavy ratios correspond to methane from known gas vents on the shelf with isotopic signatures of −28‰ PDB [*Collier and Lilley*, 2005]. The slightly lighter ratios are the result of a mixture with biogenic methane from slope seepage and/or from in situ methanogenesis in the particle-enriched layers that correlate with these shallow CH_4 maxima (see section 3.3.3). Samples with heavier isotopic signatures sometimes occur at very low CH_4 concentrations and represent residual methane left after extensive methane oxidation [*Ward and Kilpatrick*, 1993].

[32] The δ^{13}C-CH_4 ratios of surface water samples collected along a west-to-east section across the shelf edge near Newport, Oregon (seafloor depths of 420–113 m), show the importance of coastal upwelling for the transport of methane from intermediate depths to the surface and thus to the atmosphere. The isotopic ratio of methane decreases toward the shelf from −46.7 to −42.4‰ PDB at the most inshore location (113 m water depth). As the isotopic composition gets progressively heavier toward shore, the methane supersaturation and the salinity increase while the water temperature decreases. Thus the enrichment in CH_4 on the shelf results from upwelling of isotopically heavier methane, possibly from the thermogenic sources. The offshore isotopic ratios, on the contrary, were in equilibrium with the atmospheric ratios [*Holmes et al.*, 2000].

3.3. Hydrographic Controls on Methane Distributions

3.3.1. Water Masses off the Oregon Coast

[33] Through the preceding discussions of methane distributions and sources, we have clearly shown that the origin and spreading of water masses at the continental margin exerts a controlling influence on the fate of methane in this environment. Below we will review the basic distribution of water masses and the currents observed off central Oregon with a specific focus on the role of the California Undercurrent in the transport of methane from the various sources discussed above.

[34] As part of the TECFLUX field program, hydrographic surveys were carried out during the summers of 1999 and 2000. The main water masses off the Oregon margin can be recognized from the potential temperature-salinity diagram

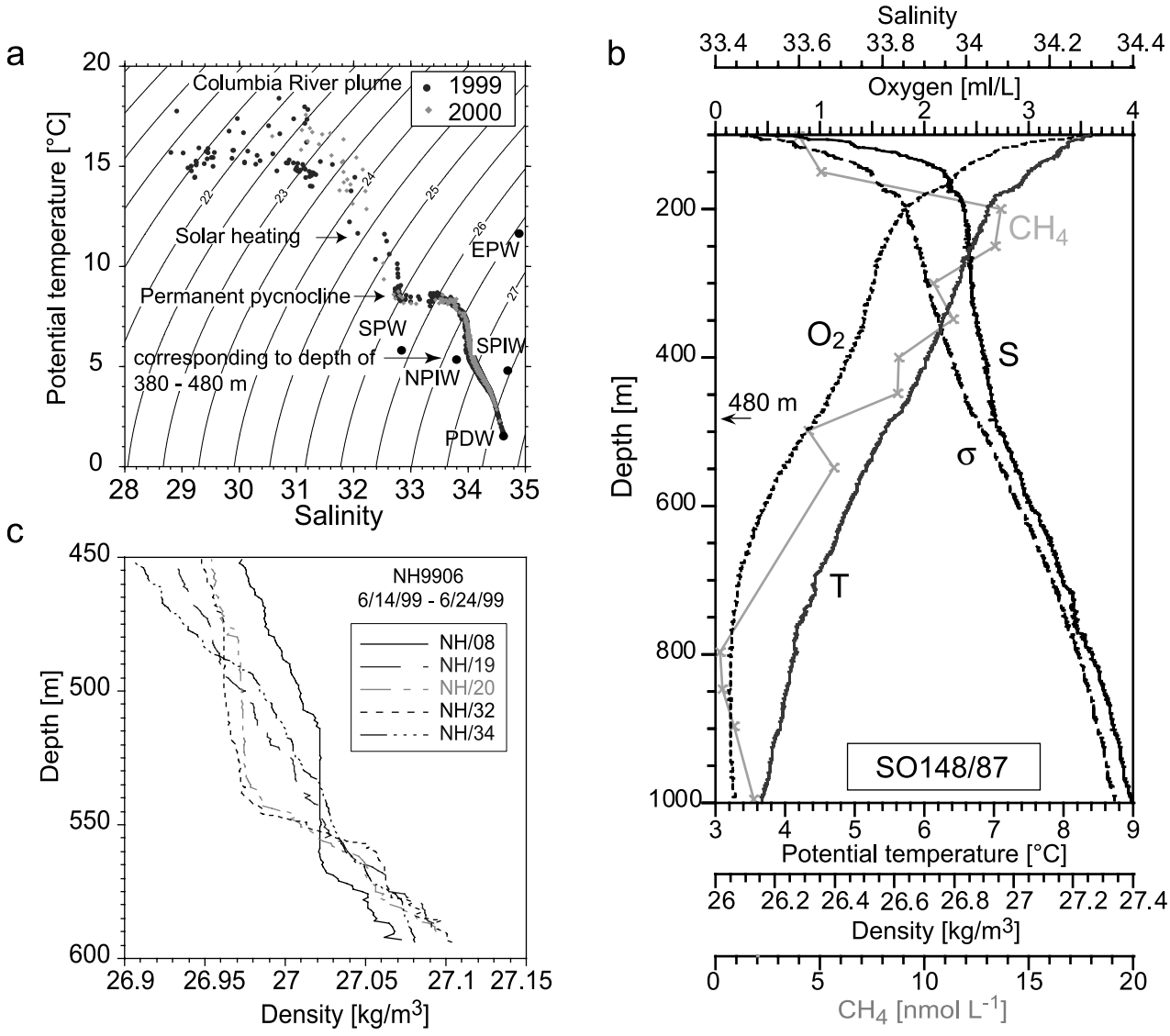

Figure 7. Hydrographic parameters for samples obtained in 1999 and 2000. (a) Water masses of the study area in a potential temperature-salinity (θ-S) diagram; dots represent the water types determining the T-S properties. See text for details. The contours indicate equal densities (σ_θ). A discontinuity in T-S properties, and thus a change in water types at depth, was found at σ = 26.85 kg m^{-3}, corresponding to depths of 430–485 m in 1999 and 380–470 m in 2000. (b) T, S, σ_θ, oxygen (O_2) and methane (CH_4) profiles of CTD station SO148/87 well represent the change in water masses at 480 m depth. (c) Density profiles of several hydrocasts taken on the cruise NH9906. These highly variable profiles were obtained within only 10 days at NHR and show rapid stratification changes implying strong mixing above Hydrate Ridge.

(Figure 7a). The warm Columbia River plume (S < 32.5) produces a shallow mixed layer in the upper 10–20 m of the water column which can be reinforced by seasonal warming. During periods of prevailing southerly winds, coastal upwelling of deeper water masses causes nearshore surface water temperatures to be colder and salinities to be higher. Below this seasonal pycnocline, a permanent halocline extends down to 120 m. The halocline is maintained by mixing of fresher, warm surface waters with Subarctic Pacific Water (SPW; σ_θ = 25.8 kg m^{-3}). The colder SPW is entrained by the shallow southward-flowing California Current jet at 48°N and transported along the coast.

[35] Below these shallower water masses, warm and saline water influenced by Equatorial Pacific Water (EPW; σ_θ = 26.6 kg m^{-3}) is transported northward by the California Undercurrent at a core depth of 200–300 m [*Tchernia*, 1980; *Lynne and Simpson*, 1987, and references therein]. The influence of the EPW decreases below the undercurrent to depths of approximately 480 m (Figure 7b), where the North Pacific Intermediate Water prevails (NPIW; σ_θ = 26.85 kg m^{-3}; S = 34.08 and T = 5.5°C) [*Talley*, 1993]. The gas hydrate-bearing vent sites are located within the NPIW where average bottom water potential temperatures were 4.65 ± 0.1°C at NHR, 4.1 ± 0.1°C at SHR, approx-

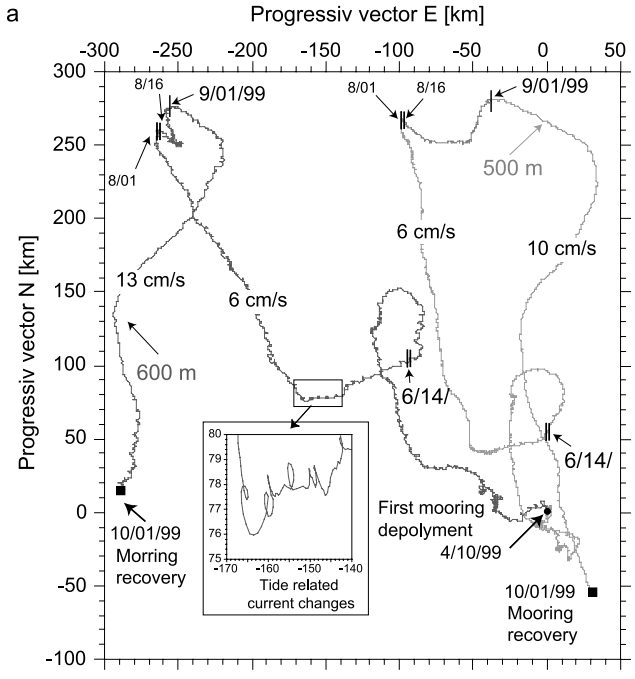

Figure 8. Progressive vector plots of current meter measurements at 500 m (shaded line) and 600 m (black line) depth starting 10 April 1999 (circle) and ending 1 October 1999 (squares). Interruptions in the plot, marked by double black lines, are due to short time recoveries. Average current speeds are given for the time period from 14 June to 1 August and 1 September to 1 October 1999. Reversal currents were observed in relation to the tidal cycle by the current meter measurements (enlargement).

imately 4.7°C at SE-Knoll, and 3.7°C at NW-Knoll. Below the NPIW, the influence of two additional water masses can be detected, the Southern Pacific Intermediate Water (SPIW; σ_θ = 27.5 kg m^{-3}) and the Pacific Deep Water (PDW; S = 34.6, T = 2°C).

3.3.2. Current Regime at Hydrate Ridge

[36] The current meter records of NHR from water depths of 500 m and 600 m yielded coherent but slightly different mean direction during a five month deployment (April–August 1999, Figure 8). At 600 m, there was a considerably stronger westward component in the currents than at 500 m. Currents at both depths showed rotation over ~30-day periods caused by mesoscale eddies. They also displayed strong oscillating tidal currents on diurnal timescales which result in complete reversals of flow. The tidal variations were also observed in bottom ADCP measurements at SHR at 790 m depth [*Linke et al.*, 2001]. These energetic near-bottom currents enhance mixing, and isopycnal layers rapidly develop and propagate through the water column above HR (Figure 7c). Rough bottom topography is known to induce stronger vertical mixing with breaking internal waves [*Ledwell et al.*, 2000] and enhanced eddy formation [*Haidvogel et al.*, 1991]. At both 500 and 600 m depths, the northward currents changed to southerly currents in early September, possibly reflecting a dynamic response to the late-season relaxation of upwelling and the coastal jet. This reversal has been observed annually in shallower shipboard ADCP data collected between 1997–1999 by *Kosro* [2002].

[37] The average current speed to transit the resultant vector between mid-June and August was 6 cm s^{-1} at both depths, whereas during September the southerly current speeds increased to 10 cm s^{-1} at 500 m and 13 cm s^{-1} at 600 m. Averaging these current speeds for the 5-month deployment yields 0.315 km h^{-1} (9 cm s^{-1}). This arithmetic average approximates the speed that water moves past HR, and can be used to estimate the residence time of water and thus the "clearing time" for methane introduced into the water column of the working area. A clearing time of 4 days

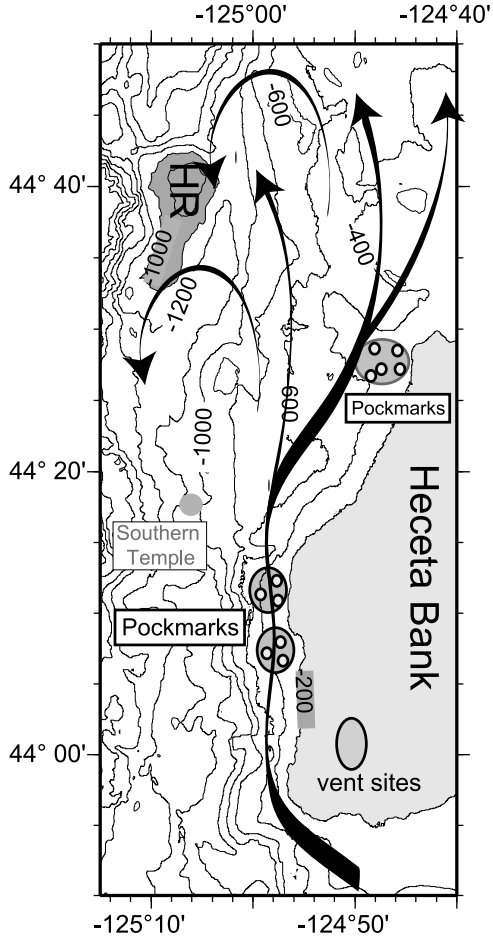

Figure 9. Sketch of possible movement of the California Undercurrent (black arrows) at the approximate latitude of HR. Pockmark fields shown in the figure were first described by *Embley et al.* [2002], while the gas vent sites on the Heceta Bank were found by *Collier and Lilley* [1995] at depth of 90 m. Currents at HR were mostly to the north and northwest but also showed eddy formation (Figure 8). As discussed in the text, the undercurrent or mesoscale eddies produced within might possibly transport methane from the sources at Heceta Bank to the region of HR causing the observed variability in methane concentration and the isotopic character above 480 m.

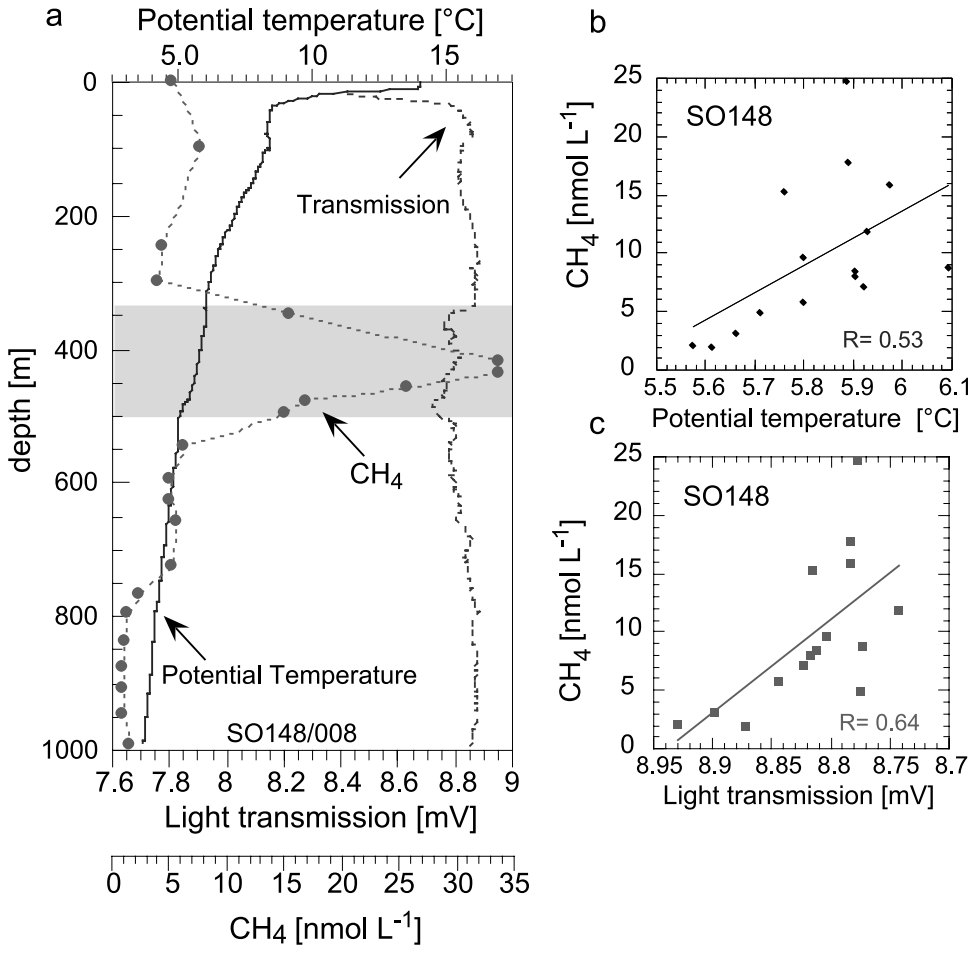

Figure 10. Intermediate nepheloid layers (INLs) at 380–480 m depth transported by the California Undercurrent. (a) Methane, temperature, and transmission profiles at station SO148/008; temperature and transmission showing discontinuities, which coincide with the depth of the methane maximum at 420 m. (b, c) Samples from SO148 at depth of 380–480 m showing correlation of elevated methane concentration with elevated temperatures and reduced light transmission, i.e., increasing numbers of particles. This correlation supports that these layers of methane maxima are INLs.

(0.01 years) is calculated by dividing the length of the working area along the main SE-NW current axis by the current speed. Although the currents are highly variable, clearly, the water masses and local chemical inputs do not remain within this section of the margin environment for very long.

3.3.3. Offshore Transport of Methane and Nepheloid Layers With the California Undercurrent

[38] As discussed above, the change in hydrographic properties, and the δ^{13}C-CH_4 composition, at around 480 m water depth represents a transition between water masses of different origin. Above this depth the water masses are transported with the California Undercurrent which flows northward hugging the continental slope, whereas the underlying NPIW is more pelagic in origin.

[39] In July 2000 an ADCP section at 44°N (GLOBEC, http:/ltop.coas.oregonstate.edu/~ctd/index.html; cited September 2004) detected the California Undercurrent at core depths of 150–400 m and with current speeds of 20 cm s^{-1} along the slope of Heceta Bank. This bank is a coastal promontory to the south-southeast of HR that can deflect the undercurrent offshore as far as 100 km into the area of Hydrate Ridge as observed in 1998 by *Kosro* [2002] (Figure 9). Gas vents, large pockmark fields, and gassy sediments that expel methane are abundant along the shelf and slope of Heceta Bank (Figure 9). The deflected California Undercurrent transports this methane and benthic nepheloid layers offshore.

[40] The origin of the shallower methane maxima from these slope areas is supported by the isotope ratios and by the correlation with a reduced light transmission and elevated temperatures (Figure 10). The last two are characteristics of detached benthic mixed layers originating from the upper slope. Transported offshore, these layers are called intermediate nepheloid layers (INLs) [e.g., *Pak et al.*, 1980; *Thorpe and White*, 1988; *Washburn et al.*, 1993; *Moum et al.*, 2002]. In addition to outside methane sources, INLs often have increased CH_4 concentrations and methane turn-

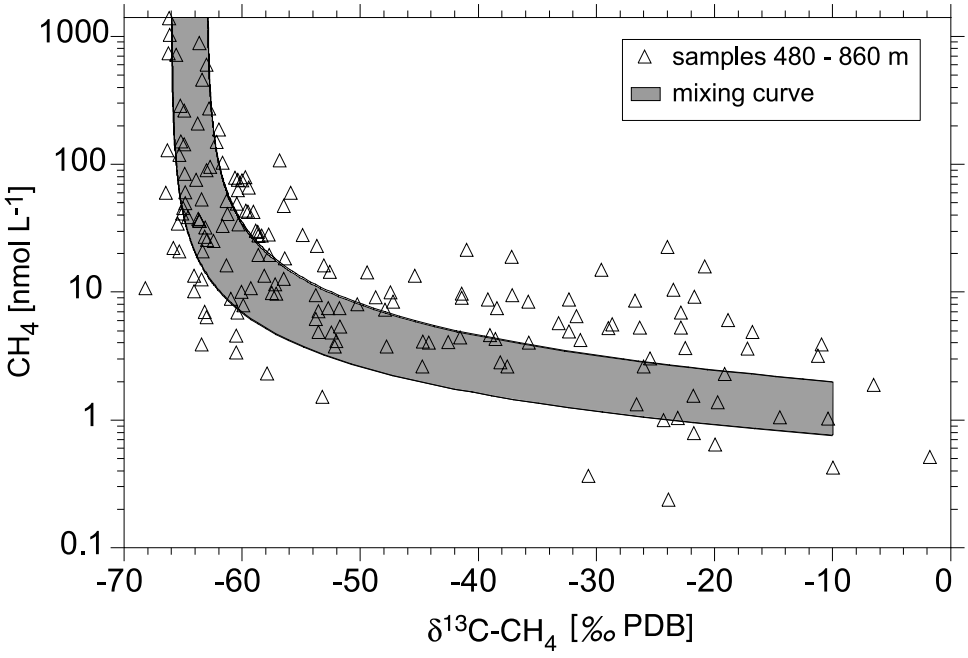

Figure 11. Three-end-member mixing. The shaded area shows the results of calculated mixing curves between the HR vent methane (1400 nmol/L and −66 to −63‰ PDB) and background values (0.75 to 2 nmol/L and −15‰ PDB). The data indicate that a third end-member (roughly 30 nmol/L and −30‰ PDB) is present above the mixing line.

overs due to a higher in situ production and an elevated number of methane oxidizers [*Ward and Kilpatrick*, 1993]. These features explain the slight deviation toward lighter isotopic ratios in the offshore maxima compared to a source of −28‰ PDB on one hand, and the heavy isotopic signatures in methane-depleted "older" INLs on the other hand (Figure 6c). The CH_4 content of the INL also varies owing to the different origins on the slope. The higher frequency of shallower CH_4 peaks in the year 2000 (SO-1, -3,-4,-5) compared to 1999 may be due to the frequent changes in the position of the California Undercurrent on the slope which were observed by *Kosro* [2002].

4. Synthesis

4.1. Controlling Features: Sources, Advection, Mixing, and Oxidation

[41] The study of the methane inputs, distributions, and isotopic compositions has identified two significant methane sources along the Oregon margin: the isotopically light CH_4 from vent sources along the accretionary complex and the isotopically heavier sources from the inshore slope. Within the water column, the fate of methane includes either dilution or microbial oxidation.

[42] The methane from below 480 m within the study site can be represented by mixtures of three end-members clearly distinguished by their $\delta^{13}C$-CH_4 compositions (Figure 11). The first end-member is the deep, isotopically light vent methane which is rapidly diluted. The second end-member represents a heavy (−25 to −6‰ PDB) "background" CH_4 component which is found offshore at low methane concentrations of 0.5 to 2 nmol L^{-1}. Most of the methane variations at these depths can be well represented by the mixtures of these two end-members, falling along the shaded mixing curves in Figure 11. Only samples in the 5–15 nmol L^{-1} concentration range, which originate closer to the slope, lie above these binary mixtures and show an additional influence of the third isotopically heavier sources on the slope. There is enough scatter in the intermediate-to-low concentration range of the deep water $\delta^{13}C$-CH_4 ratios that one cannot graphically distinguish the impact of methane oxidation from binary mixing.

[43] The isotopically heavy background CH_4 likely is the unoxidized residual of methane introduced elsewhere along the continental margin which is advected into the vicinity of HR. This conclusion is supported by relatively short residence times of the water on the margin and methane oxidation rates of only 0.09 to 4.1% per day. These rates were determined in water samples above HR which were incubated with ^{14}C (for methods, see *de Angelis et al.* [1993]). These oxidation rates equal a microbial oxidation turnover time of 0.07 to 3.2 years. At an advective "clearing time" of about 0.01 years, the methane oxidation can therefore only account for a maximum CH_4 decrease of 14% in the entire working area. Thus our data clearly suggest that dilution is primarily responsible for the observed decrease in CH_4 concentrations and that oxidation is only important on longer temporal and spatial scales. Models concerning methane oxidation at continental margins [e.g., *Valentine et al.*, 2001; *Grant and Whiticar*, 2002] should therefore integrate the advection of isotopically heavy "background water." This is especially true if look-

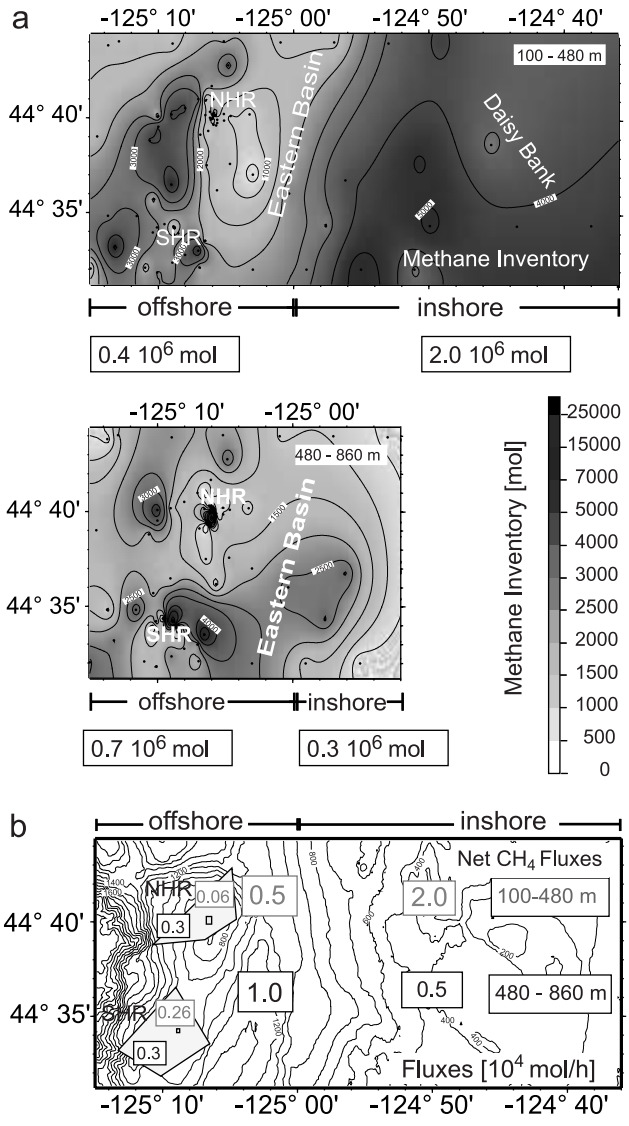

Figure 12. Distribution of methane sources in the study area showing (a) inventories and (b) calculated methane fluxes. For these estimates, seven boxes were considered: the total working area, one offshore and one inshore box, one NHR and SHR sub-region (gray box), and one NHR and SHR vent region (small rectangle within sub-regions). Each box consists of a shallow range of 100–480 m (upper panel in Figure 12a and shaded numbers in Figure 12b) and a deep range of 480–860 m (lower panel in Figure 12a and black numbers in Figure 12b). The deeper Eastern Basin (125°W) was set as the arbitrary boundary separating inshore waters from offshore waters. All methane inventories and methane flux estimates are also listed in Table 2.

ing at small temporal and spatial scales. Possible additional methane sources should be discussed in any case.

4.2. Methane Inventory and Fluxes

[44] Because of the large number of sources and the complexity of the hydrography along the Cascadia margin, it was not possible to simply calculate fluxes through constrained volumes, a method that has been successful for deep hydrothermal plumes [*Kadko et al.*, 1990; *Lavelle et al.*, 1998]. Instead, a first-order estimate was made by calculating the total excess methane inventories in subregions of the margin and assuming that these must be replenished over a defined clearing time estimated from measured currents. Calculation of the inventory allows us to compare the relative significance of primary sources across the margin, and the resulting flux estimates can be compared with direct estimates from the vent sites and fluxes from other marine environments.

[45] We divided the study site into shallow/deep and inshore/offshore boxes that were well constrained by our samples (Figure 12). The north-south boundaries of the volume were defined to include the NH-1 and NH-2 sections (Figure 1) over a total depth range of 100–860 m. In order to separate the influence of upper slope sources from those related to gas hydrate-bearing sediments, the upper and lower boxes were divided at 480 m depth. The inshore slope/shelf sources were most effectively separated from the offshore accretionary complex sources including Hydrate Ridge, by a division at 125°W. In order to better reflect the fluxes from the known sources on HR (and supported by the larger number of profiles collected there), two nested sub-regions were defined around each summit. NHR and SHR sub-region inventories contained all CTD profiles between the sections SO-1 to SO-2 and SO-3 to SO-4, respectively (see Figures 1 and 12b). Inner, vent-focused boxes at NHR and SHR included all profiles within a small polygon that surrounded any profile with CH_4 concentrations greater than 100 nmol L^{-1}. These areas were approximately 200 m in diameter around SHR and 700 m in diameter around NHR which included at least three separate vent sources.

[46] For each of these sub-regions, methane concentrations were integrated through the appropriate depth range within each CTD profile, and background concentrations were removed. The latter were estimated from the farthest offshore profiles collected over the Western Basin. These were 3.4 nmol L^{-1} for samples shallower than 480 m and 0.6 nmol L^{-1} for deeper samples. The resulting "excess" CH_4 inventories for each profile were gridded (Figure 12a), and these were integrated to arrive at an inventory for each sub-region. To the extent that this inventory represents "new methane" added within the control volumes and that currents continuously sweep through these volumes, we can make first-order estimates of the input flux of methane needed to support these inventories (Table 2). For the currents that "clear" the observed methane from the control volumes, we have chosen a mean speed of 9 cm s^{-1} which was determined in the deep box at NHR (see section 3.3). This current speed is consistent with the mean of the maximum velocity at 325 m as determined from an extensive ADCP data set in summer 1995 [*Pierce et al.*, 2000]. This data set includes cross-shore sections along the west American coast that reach from the shelf to a distance of 50 km offshore. For the depth-averaged layer from 125 to 325 m a mean of the maximum velocity was 0.18 ± 0.01 m s^{-1}. The applied clearing time might thus be slightly under-

Table 2. Methane Excess Inventories and Methane Fluxes of the Hydrate Ridge Area

Region	Area, km^2	Excess CH_4 Inventory, mol	Clearing Time,[a] hours	Net CH_4 Flux, mol h^{-1}	Area-Normalized CH_4 Flux, mmol m^{-2} d^{-1}
		100–480 m Depth			
Total	1231	$2.4 \cdot 10^6$	95	$2.5 \cdot 10^4$	0.5
West of 125	472	$0.4 \cdot 10^6$	70	$0.5 \cdot 10^4$	0.3
East of 125	758	$2.0 \cdot 10^6$	88	$2.2 \cdot 10^4$	0.6
		480–860 m Depth			
Total	734	$1.0 \cdot 10^6$	74	$1.4 \cdot 10^4$	0.5
West of 125	472	$0.7 \cdot 10^6$	70	$1.0 \cdot 10^4$	0.5
East of 125	261	$0.3 \cdot 10^6$	56	$0.5 \cdot 10^4$	0.5
		100–480 m Depth			
NHR subregion	47	$1.3 \cdot 10^4$	22	$0.6 \cdot 10^3$	0.3
SHR subregion	37	$5.8 \cdot 10^4$	22	$2.6 \cdot 10^3$	1.7
		480–860 m Depth			
NHR subregion	47	$8.3 \cdot 10^4$	22	$3.8 \cdot 10^3$	1.9
SHR subregion	37	$5.7 \cdot 10^4$	22	$2.6 \cdot 10^3$	1.7
NHR vent box	0.376	1042	2	532	34
SHR vent box	0.029	218	0.5	400	328

[a]Changes in clearing times result from different box geometries.

estimated for the shallower inshore box where the core of the California Undercurrent should be found. Further errors in this analysis result from the single inventory for each control volume in this variable system and from the rough assumption concerning methane that is transported into the control volumes through their boundaries. Therefore we assume the final estimates to represent the order of magnitude of the methane fluxes.

[47] The total methane flux over all depths between 100 and 860 m was approximately 4×10^4 mol h^{-1}, of which 40% came from sources within the GHSZ, i.e., at depths below 480 m. Because of the difference in box sizes, the area-normalized methane fluxes above and below the GHSZ are approximately the same (0.5 mmol m^{-2} d^{-1}) (Table 2). Within the GHSZ, CH_4 fluxes (0.5 mmol m^{-2} d^{-1}) are the same in the inshore area east of 125°W and in the offshore area where Hydrate Ridge and its gas vents are located. This suggests that strong methane venting is not restricted to Hydrate Ridge, but rather is a common occurrence along the accretionary wedge of the Cascadia Margin. In spite of the significance of shallower sources, the methane flux from the deeper gas hydrate-bearing sediments is a substantial fraction of the total budget from the margin.

[48] Within the shallower volume above the GHSZ, about 80% of the methane inventory is contained in the inshore area where the shelf/slope methane sources are located. Nevertheless, over SHR, shallow and deep methane fluxes were equivalent, although not from the same source. This emphasizes the significance of offshore transport by the California Current system to the shallower box. Many of the samples in the SHR sub-region inventories were collected in the year 2000 when transport by the California Current was stronger.

[49] The methane fluxes from the deep sub-regions of NHR and SHR each account for approximately 0.3×10^4 mol CH_4 h^{-1}. This is comparable to the CH_4 gas flux of 0.25×10^4 mol h^{-1} estimated by *Torres et al.* [2002] for the strongest venting area at NHR. The order-of-magnitude difference in the area-normalized flux at the inner, vent-focused boxes at SHR and NHR is because the three vent sources included in the NHR vent box are spread over a wider area [*Heeschen et al.*, 2003]. In contrast, all the profiles at SHR focus on the single vent site.

[50] The methane flux of 328 mmol m^{-2} d^{-1} from the SHR vent box primarily reflects methane gas ebullition and could be compared to flux estimates for methane transported via vent fluids into the bottom water at SHR of 100 mmol m^{-2} d^{-1} [*Boetius et al.*, 2000; *Torres et al.*, 2002]. However, this fluid flow is restricted to regions covered with bacterial mats, an area of roughly 100 m^2 [*Tryon et al.*, 2002]. The area of the SHR vent box is 3×10^4 m^2 such that the total methane flux estimate is about 2 orders of magnitude larger than the fluid flow. This difference further emphasizes the importance of the gas phase fluxes into the water column compared to the transport of CH_4 via fluid flow.

[51] The methane fluxes estimated for the various subsections of the Cascadia Margin and HR vent sources can be compared with fluxes from other marine methane sources. Specifically, the estimates for the deep HR sub-regions (0.3×10^4 mol h^{-1}, Table 2) can be compared to fluxes found at some other well-characterized gas seeps. For example, a flux of 0.4×10^4 mol h^{-1} has been estimated for the Tommeliten field in the northern North Sea (120 bubble plumes, 70 m water depth, area of 6.5 km^2 [*Hovland et al.*, 1993]). The methane fluxes of 15×10^4 mol CH_4 h^{-1} enter the water column at the Coal Point Oil seeps on the California shelf, which are the strongest natural gas seeps known [*Clark et al.*, 2000]. Marine hydrothermal systems also release methane to the deep ocean, and a flux of 1.6×10^4 mol h^{-1} has been estimated for the main Endeavour Ridge vent system [*Rosenberg et al.*, 1988; *Kadko et al.*, 1990]. The total deep, hydrate-bearing section of the Cascadia Margin produces 1.5×10^4 mol CH_4 h^{-1}, and the full marine section flux is approximately 4×10^4 mol h^{-1}. This flux already accounts

for about 0.01–0.7% of the present estimates for global natural methane emissions from marginal seabeds to the hydrosphere and atmosphere [*Hovland et al.*, 1993; *Judd*, 2000; *Judd et al.*, 2002; *Kvenvolden et al.*, 2001]. Thus our results support recent statements about the importance of the continental margins for the methane cycle [e.g., *Judd et al.*, 2002].

5. Conclusions

[52] The multiyear survey of the methane distributions in the water column at Hydrate Ridge revealed a complex system which is controlled by numerous sources. In the gas hydrate stability zone, the main fluxes reflect methane gas phase input. The timing of this methane gas ebullition is different between Southern and Northern Hydrate Ridge. The isotope ratio of water column methane is close to the stable carbon isotope ratios of vent gas methane at SHR (−66‰ PDB) and NHR (−63‰ PDB). Other source areas within the gas hydrate stability zone have δ^{13}C-CH_4 signatures in the range of −58 to −72‰ PDB. Above 480 m depth, the methane inventory is determined by the offshore transport of isotopically heavier methane from various sources on the upper slope and shelf by the energetic California Current system. The isotopic ratios at these depths vary between −56 to −28‰ PDB with a peak at about −30‰ PDB.

[53] The California Current system, with frequent mesoscale eddies and current variability over a range of timescales (tidal to interannual), results in the rapid mixing of methane away from these sources. The resulting methane found along the margin can be understood in terms of the mixing of three end-members, which can be distinguished by their δ^{13}C-CH_4 signatures: (1) a deep, isotopically light source at HR; (2) a shallow thermogenic source near −30‰ PDB; and (3) a very heavy, low-methane "background" component ranging up to −6‰ PDB. The heavy isotope ratios for the background methane and the relatively large scatter in the isotopic values around the mixing curves at low concentrations are evidence for isotope fractionation driven by methane oxidation. However, the "clearing time" of the margin section, estimated from current observations, is much less than the time needed to oxidize the methane to background levels. We did not observe the direct ascent of methane gas to the surface.

[54] Calculations showed that the methane flux originating on the upper continental slope and from shelf sources is twice as high (2×10^4 mol h^{-1}) as the flux from the hydrate-related sources below 480 m. However, due to the smaller size of the deep water region, methane flux per area (0.5 mmol m^{-2} d^{-1}) is about the same in the water column above and below the hydrate stability zone boundary. In conclusion, the methane flux from accretionary wedges must be considered when oceanic methane budgets are assessed.

[55] **Acknowledgments.** We greatly appreciate the support at sea by the masters and crews of R/V *Ron Brown*, R/V *New Horizon*, R/V *Atlantis*, R/V *Sonne*, and R/V *Wecoma*. We thank Julie Arrington, Barbara Bock, Magnus Eek, Nick Grant, Ulrich Kunz, Hinrich Schaefer, and Andrea Voorhees for their indispensable help at sea. Special thanks go to Michael Whiticar, Paul Eby, Hinrich Schaefer, and Nick Grant for their support at SEOS. For helpful comments on the manuscript we thank Robin Keir, Marta Torres, Sarah Hoffman, and Wolfgang Hukriede. Financial support for this work was granted by the National Science Foundation (OCE-9731157; OCE-9811471 and OCE-973123) and the German Federal Ministry of Education and Research (BMBF, Fkz 03G0143A and 03GO148A). This is publication GEOTECH-40 of the program GEOTECHNOLOGIEN of the BMBF and the Deutsche Forschungsgemeinschaft (DFG).

References

Barth, J. A., S. D. Pierce, and R. L. Smith (2000), A separating coastal upwelling jet at Cape Blanco, Oregon and its connection to the California Current System, *Deep Sea Res.*, *47*, *Part II*, 783–810.

Bates, T. S., K. C. Kelly, J. E. Johnson, and R. H. Gammon (1996), A reevaluation of the open ocean source of methane to the atmosphere, *J. Geophys. Res.*, *101*(D3), 6953–6961.

Boetius, A., K. Ravenschlag, C. J. Schubert, D. Rickert, F. Widdel, A. Giesecke, R. Amann, B. B. Jorgensen, U. Witte, and O. Pfannkuche (2000), A marine microbial consortium apparently mediating anaerobic oxidation of methane, *Nature*, *407*, 623–626.

Bohrmann, G., J. Greinert, E. Suess, and M. E. Torres (1998), Authigenic carbonates from the Cascadia subduction zone and their relation to gas hydrate stability, *Geology*, *26*, 647–650.

Bohrmann, G., P. Linke, E. Suess, O. Pfannkuche, and shipboard party (1999), RV *Sonne* cruise report SO143, TECFLUX-I-1999, *Rep. 93*, 217 pp., GEOMAR, Kiel, Germany.

Cicerone, R. J., and R. S. Oremland (1988), Biogeochemical aspects of atmospheric methane, *Global Biogeochem. Cycles*, *2*(4), 299–327.

Clark, J. F., L. Washburn, J. S. Hornafius, and B. P. Luyendyk (2000), Dissolved hydrothermal flux from natural marine seeps to the southern California Bight, *J. Geophys. Res.*, *105*(C5), 11,509–11,522.

Collier, R. W., and M. Lilley (1995), Geochemistry of gases and fluids from seeps on the S. Oregon continental shelf, paper presented at Annual Meeting 20, Geol. Assoc. of Can., Victoria, B. C., Canada.

Collier, R. W., and M. Lilley (2005), Composition of shelf methane seeps on the Cascadia Continental Margin, *Geophys. Res. Lett.*, *32*, L06609, doi:10.1029/2004GL022050.

Collins, C. A., N. Garfield, R. G. Paquette, and E. Carter (1996), Lagrangian measurements of subsurface poleward flow between 38°N and 43°N along the west coast of the United States during summer, 1993, *Geophys. Res. Lett.*, *23*(18), 2461–2464.

Damm, E., and G. Budéus (2003), Fate of vent-derived methane in seawater above the Håkon Mosby mud volcano (Norwegian Sea), *Mar. Chem.*, *82*, 1–11.

de Angelis, M. A., M. D. Lilley, E. J. Olson, and J. A. Baross (1993), Methane oxidation in deep-sea hydrothermal plumes of the Endeavour segment of the Juan de Fuca Ridge, *Deep Sea Res., Part I*, *40*, 1169–1186.

DeMets, C., G. R. Gordon, D. F. Argus, and S. Stein (1990), Current plate motions, *Geophys. J. Int.*, *101*, 425–478.

Dickens, G. R. (2003), Rethinking the global carbon cycle with a large, dynamic and microbially mediated gas hydrate capacitor, *Earth Planet. Sci. Lett.*, *213*, 169–183.

Dickens, G. R., and M. S. Quinby-Hunt (1994), Methane hydrate stability in seawater, *Geophys. Res. Lett.*, *21*(19), 2115–2118.

Dickens, G. R., J. R. O'Neil, D. K. Rea, and R. M. Owen (1995), Dissociation of oceanic methane hydrate as a cause of the carbon isotope excursion at the end of the Paleocene, *Paleoceanography*, *10*(6), 963–971.

Duan, Z., N. Moller, J. Greenberg, and J. H. Weare (1992), The prediction of methane solubility in natural waters to high ionic strength from 0 to 250 degrees C and from 0 to 1600 bar, *Geochim. Cosmochim. Acta*, *56*(4), 1451–1460.

Elvert, M., E. Suess, J. Greinert, and M. Whiticar (2000), Archaea mediating anaerobic methane oxidation in deep-sea sediments at cold seeps of the eastern Aleutian subduction zone, *Org. Geochem.*, *31*(11), 1175–1187.

Embley, R. W., W. Wakefield, S. G. Merle, A. Valdes, and G. Hendler (2002), Pockmarks, seeps, and carbonates on Heceta Bank and its seaward slope, *Geol. Soc. Am. Abstr. Programs*, *34*(5), 42.

Etheridge, D. M., G. I. Pearman, and P. J. Fraser (1992), Changes in tropospheric methane between 1841 and 1978 from a high accumulation-rate Antarctic ice core, *Tellus, Ser. B*, *44*, 282–294.

Garfield, N., C. A. Collins, R. G. Paquette, and E. Carter (1999), Lagrangian exploration of the California Undercurrent, 1992–1995, *J. Phys. Oceanogr.*, *29*, 560–583.

Gornitz, V., and I. Fung (1994), Potential distribution of methane hydrates in the world's oceans, *Global Biogeochem. Cycles*, *8*(3), 335–347.

Grant, N. J. (2000), Stable carbon isotopic evidence for bacterial oxidation and mixing in two deep-sea methane plumes, M. Sc., 188 pp., Univ. of Victoria, Victoria, B. C., Canada.

Grant, N. J., and M. J. Whiticar (2002), Stable carbon isotopic evidence for methane oxidation in plumes above Hydrate Ridge, Cascadia Oregon margin, *Global Biogeochem. Cycles*, *16*(4), 1124, doi:10.1029/2001GB001851.

Grasshoff, M., K. Ehrhardt, and K. Kremling (1983), *Methods of Seawater Analysis*, 419 pp., Verlag Chemie, Weinheim, Germany.

Greinert, J., G. Bohrmann, and E. Suess (2001), Gas hydrate-associated carbonates and methane-venting at Hydrate Ridge: Classification, distribution, and origin of authigenic lithologies, in *Natural Gas Hydrates: Occurrence, Distribution, and Detection*, *Geophys. Monogr. Ser.*, vol. 124, edited by C. K. Paull and W. P. Dillon, pp. 99–113, AGU, Washington, D. C.

Haidvogel, D. B., A. Beckmann, and K. S. Hedström (1991), Dynamical simulations of filament formation and evolution in the coastal transition zone, *J. Geophys. Res.*, *96*(C8), 15,017–15,040.

Heeschen, K. U., A. M. Tréhu, R. W. Collier, E. Suess, and G. Rehder (2003), Distribution and height of methane bubble plumes on the Cascadia margin characterized by acoustic imaging, *Geophys. Res. Lett.*, *30*(12), 1643, doi:10.1029/2003GL016974.

Hesselbo, S. P., D. R. Gröcke, H. C. Jenkyns, C. J. Bjerrum, R. Farrimond, H. S. Morgans Bell, and O. R. Green (2000), Massive dissociation of gas hydrate during a Jurassic oceanic anoxic event, *Nature*, *406*, 392–395.

Holmes, M. E., F. J. Sansone, T. M. Rust, and B. N. Popp (2000), Methane production, consumption, and air-sea exchange in the open ocean: An evaluation based on carbon isotopic ratios, *Global Biogeochem. Cycles*, *14*(1), 1–10.

Hornafius, J. S., D. Quigley, and B. P. Luyendyk (1999), The world's most spectacular marine hydrocarbon seeps (Coal Oil Point, Santa Barbara Channel, California): Quantification of emission, *J. Geophys. Res.*, *104*(C9), 20,703–20,711.

Hovland, M., A. G. Judd, and R. A. J. Burke (1993), The global flux of methane from shallow submarine sediments, *Chemosphere*, *26*, 559–578.

Huyer, A. (1977), Seasonal variation in temperature, salinity, and density over the continental shelf off Oregon, *Limnol. Oceanogr.*, *22*(3), 442–453.

Huyer, A. (1983), Coastal upwelling in the California Current System, *Prog. Oceanogr.*, *12*, 259–284.

Huyer, A., E. J. C. Sobey, and R. L. Smith (1979), The spring transition in currents over the Oregon continental shelf, *J. Geophys. Res.*, *84*(C11), 6995–7011.

Huyer, A., P. M. Kosro, J. Fleischbein, S. R. Ramp, T. Stanton, L. Washburn, F. P. Chavez, T. J. Cowles, S. D. Pierce, and R. L. Smith (1991), Currents and water masses of the Coastal Transition Zone off Northern California, June to August 1988, *J. Geophys. Res.*, *96*(C8), 14,809–14,831.

Huyer, A., J. A. Barth, P. M. Kosro, R. K. Shearman, and R. L. Smith (1998), Upper-ocean water mass characteristics of the California current, Summer 1993, *Deep Sea Res., Part II*, *45*, 1411–1442.

Johnson, J. E., C. Goldfinger, and A. M. Tréhu (2000), Structural development and deformation styles of the Hydrate Ridge region, Cascadia accretionary prism, *Geol. Soc. Am. Abstr. Programs*, *32*(7), 36.

Johnson, J. E., C. Goldfinger, and E. Suess (2003), Geophysical constraints on the surface distribution of authigenic carbonates across the Hydrate Ridge region, Cascadia Margin, *Mar. Geol.*, *202*(1–2), 79–120.

Judd, A. G. (2000), Geological sources of methane, in *Atmospheric Methane: Its role in the Global Environment*, edited by M. A. K. Khalili, pp. 280–303, Springer, New York.

Judd, A. G., M. Hovland, L. I. Dimitrov, S. García Gil, and V. Jukes (2002), The geological methane budget at continental margins and its influence on climate change, *Geofluids*, *2*, 109–126.

Kadko, D. C., N. D. Rosenberg, J. E. Lupton, W. R. Collier, and M. D. Lilley (1990), Chemical reaction rates and entrainment within the Endeavor Ridge hydrothermal plume, *Earth Planet. Sci. Lett.*, *99*, 315–335.

Karl, D. M., and B. D. Tilbrook (1994), Production and transport of methane in oceanic particulate organic matter, *Nature*, *368*, 732–734.

Kasting, J. F., and J. L. Siefert (2002), Life and the evolution of Earth's atmosphere, *Science*, *296*, 1066–1068.

Kastner, M., K. A. Kvenvolden, and T. D. Lorenson (1998), Chemistry, isotopic composition, and origin of a methane-hydrogen sulfide hydrate at the Cascadia subduction zone, *Earth Planet. Sci. Lett.*, *156*, 173–183.

Kennedy, M. J., N. Christie-Blick, and L. E. Sohl (2001), Are Proterozoic cap carbonates and isotopic excursions a record of gas hydrate destabilization following Earth's coldest intervals?, *Geology*, *29*, 443–446.

Kennett, J. P., K. G. Cannariato, I. H. Hendy, and R. J. Behl (2000), Carbon isotopic evidence for methane hydrate instability during Quaternary interstadials, *Science*, *288*, 128–133.

Kennett, J. P., K. G. Cannariato, I. L. Hendy, and R. J. Behl (2003), *Methane Hydrates in Quaternary Climate Change: The Clathrate Gun Hypothesis*, 216 pp., AGU, Washington, D. C.

Klinkhammer, G. P., and J. McManus (2001), Dissolved manganese in the Columbia River estuary: Production in the water column, *Geochim. Cosmochim. Acta*, *65*(17), 2835–2841.

Klinkhammer, G., R. W. Collier, P. Linke, F. Appel, K. Heeschen, E. Suess, M. A. de Angelis, M. Masson, and S. Marx (1999), Applications of the METS methane sensor to the in situ detection of methane over a range of time scales and environments, *Eos Trans. AGU*, *80*(46), Fall Meet. Suppl., F510.

Kosro, P. M. (2002), A poleward jet and an equatorward undercurrent observed off Oregon and northern California, during the 1997–1998 El Niño, *Prog. Oceanogr.*, *54*, 343–360.

Kosro, P. M., and A. Huyer (1986), CTD and velocity surveys of seaward jets off northern California, July 1981 and 1982, *J. Geophys. Res.*, *91*(C6), 7680–7690.

Kosro, P. M., et al. (1991), The structure of the transition zone between coastal waters and the open ocean off northern California, winter and spring, 1987, *J. Geophys. Res.*, *96*(C8), 14,707–14,730.

Kulm, L. D., et al. (1986), Oregon subduction zone: venting, fauna and carbonates, *Science*, *231*, 561–566.

Kvenvolden, K. A. (1988), Methane hydrate—A major reservoir of carbon in the shallow geosphere, *Chem. Geol.*, *71*, 41–51.

Kvenvolden, K. A. (1993), Gas hydrates: Geological perspective and global changes, *Rev. Geophys.*, *31*, 173–187.

Kvenvolden, K. A. (1999), Potential effects of gas hydrate on human welfare, *Proc. Natl. Acad. Sci.*, *96*, 3420–3426.

Kvenvolden, K. A. (2002), Methane hydrate in the global organic carbon cycle, *Terra Nova*, *14*, 302–306.

Kvenvolden, K. A., W. S. Reeburgh, and T. D. Lorenson (2001), Naturally occurring methane seepage as a factor in global climate change, paper presented at USGS Workshop, U.S. Geol. Soc., Portland, Oreg.

Lammers, S., and E. Suess (1994), An improved head-space analysis method for methane in seawater, *Mar. Chem.*, *47*, 115–125.

Lavelle, J. W., E. T. Baker, and G. J. Massoth (1998), On the calculation of total heat, salt and tracer fluxes from ocean hydrothermal events, *Deep Sea Res., Part II*, *45*, 2919–2936.

Ledwell, J. R., E. T. Montgomery, K. L. Polzin, L. C. St. Laurent, R. W. Schmitt, and J. M. Toole (2000), Evidence for enhanced mixing over rough topography in the abyssal ocean, *Nature*, *403*, 179–182.

Leifer, I., and A. G. Judd (2002), Oceanic methane layers: the hydrocarbon seep bubble deposition hypothesis, *Terra Nova*, *14*, 417–424.

Leifer, I., and R. K. Patro (2002), The bubble mechanism for methane transport from the shallow sea bed to the surface: A review and sensitivity study, *Cont. Shelf Res.*, *22*, 2409–2428.

Leifer, I., J. F. Clark, and R. F. Chen (2000), Modifications of the local environment by natural marine hydrocarbon seeps, *Geophys. Res. Lett.*, *27*(22), 3711–3714.

Lelieveld, J., P. J. Crutzen, and C. Brühl (1993), Climate effects of atmospheric methane, *Chemosphere*, *26*, 739–768.

Lelieveld, J., P. J. Crutzen, and F. J. Dentener (1998), Changing concentration, lifetime and climate forcing of atmospheric methane, *Tellus, Ser. B*, *50*, 128–150.

Linke, P., E. Suess, M. E. Torres, V. Martens, W. D. Rugh, W. Ziebis, and L. D. Kulm (1994), In situ measurements of fluid flow from cold seeps at active continental margins, *Deep Sea Res., Part I*, *41*, 721–739.

Linke, P., E. Suess, and shipboard members (2001), RV *Sonne* cruise report SO148, TECFLUX-II-2000, *Rep. 98*, 122 pp., GEOMAR, Kiel, Germany.

Luff, R., and K. Wallmann (2003), Fluid flow, methane flux, carbonate precipitation and biogeochemical turnover in gas hydrate–bearing sediments at Hydrate Ridge, Cascadia Margin: Numerical modeling and mass balances, *Geochim. Cosmochim. Acta*, *67*(18), 3403–3421.

Lynne, R. L., and J. J. Simpson (1987), The California Current System: The seasonal variability of its physical characteristics, *J. Geophys. Res.*, *92*(C12), 12,947–12,966.

MacDonald, G. (1990), Role of methane clathrates in past and future climates, *Clim. Change*, *16*, 247–281.

MacKay, M. E., G. R. Moore, G. R. Cochrane, J. C. Moore, and L. D. Kulm (1992), Landward vergence and oblique structural trends in the Oregon margin accretionary prism: Implications and effect on fluid flow, *Earth Planet. Sci. Lett.*, *109*, 477–491.

MacKay, M. E., R. D. Jarrad, G. K. Westbrook, R. D. Hyndman, and Shipboard Scientific Party of ODP Leg 146 (1994), Origin of bottom-

simulating reflector: Geophysical evidence from the Cascadia accretionary prism, *Geology*, *22*, 459–462.
McDougall, T. J. (1978), Bubble plumes in stratified environments, *J. Fluid Mech.*, *85*(4), 655–672.
Merritt, D. A., J. M. Hayes, and D. J. DesMarais (1995), Carbon isotopic analysis of atmospheric methane by isotope-ratio-monitoring gas chromatography-mass spectrometry, *J. Geophys. Res.*, *100*(D1), 1317–1326.
Milkov, A. V. (2004), Global estimates of hydrate-bound gas in marine sediments: How much is really out there?, *Earth Sci. Rev.*, *66*(3–4), 183–197.
Moum, J. N., D. R. Caldwell, J. D. Nash, and G. D. Gunderson (2002), Observations of boundary mixing over the continental slope, *J. Phys. Oceanogr.*, *32*, 2113–2130.
Pak, H., R. J. V. Zaneveld, and J. Kitchen (1980), Intermediate nepheloid layers observed off Oregon and Washington, *J. Geophys. Res.*, *85*(C), 6697–6708.
Pierce, S. D., R. L. Smith, P. M. Kosro, J. A. Barth, and C. D. Wilson (2000), Continuity of the poleward undercurrent along the eastern boundary of the mid-latitude north Pacific, *Deep Sea Res., Part II*, *47*, 811–829.
Rehder, G., R. S. Keir, E. Suess, and M. Rhein (1999), Methane in the northern Atlantic controlled by microbial oxidation and atmospheric history, *Geophys. Res. Lett.*, *26*(5), 587–590.
Rehder, G., R. W. Collier, K. U. Heeschen, P. M. Kosro, J. A. Barth, and E. Suess (2002a), Enhanced marine CH_4 emission to the atmosphere off Oregon caused by coastal upwelling, *Global Biogeochem. Cycles*, *16*(3), 1081, doi:10.1029/2000GB001391.
Rehder, G., P. G. Brewer, E. T. Peltzer III, and G. Friederich (2002b), Enhanced lifetime of methane bubble streams within the deep ocean, *Geophys. Res. Lett.*, *29*(15), 1731, doi:10.1029/2001GL013966.
Rosenberg, N., J. E. Lupton, D. Kadko, R. W. Collier, M. D. Lilley, and H. Pak (1988), Estimation of heat and chemical fluxes from a seafloor hydrothermal vent field using radon measurements, *Nature*, *334*, 604–607.
Sahling, H., D. Rickert, R. Lee, P. Linke, and E. Suess (2002), Macrofaunal community structure and sulfide flux at gas hydrate deposits from the Cascadia convergent margin, NE Pacific, *Mar. Ecol. Prog. Ser.*, *231*, 121–138.
Strub, P. T., P. M. Kosro, A. Huyer, and CTZ Collaborators (1991), The nature of cold filaments in the California Current system, *J. Geophys. Res.*, *96*(C8), 14,743–14,768.
Suess, E., et al. (1999), Gas hydrate destabilization: enhanced dewatering, benthic material turnover and large methane plumes at the Cascadia convergent margin, *Earth Planet. Sci. Lett.*, *170*, 1–15.
Suess, E., et al. (2001), Sea floor methane hydrates at Hydrate Ridge, Cascadia margin, in *Natural Gas Hydrates: Occurrence, Distribution, and Detection*, *Geophys. Monogr. Ser.*, vol. 124, edited by C. K. Paull and W. P. Dillon, pp. 87–98, AGU, Washington, D. C.
Talley, L. D. (1993), Distribution and formation of the North Pacific Intermediate Water, *J. Phys. Oceanogr.*, *23*, 517–527.
Tchernia, P. (1980), *Descriptive Regional Oceanography*, 253 pp., Elsevier, New York.
Teichert, B. M. A., A. Eisenhauer, G. Bohrmann, A. Haase-Schramm, B. Bock, and P. Linke (2003), U/Th systematics and ages of authigenic carbonates from Hydrate Ridge, Cascadia Margin: recorders of fluid flow variations, *Geochim. Cosmochim. Acta*, *67*(20), 3845–3857.
Thorpe, S. A., and M. White (1988), A deep intermediate nepheloid layer, *Deep Sea Res., Part I*, *35*(9), 1665–1671.
Torres, M. E., K. Brown, R. W. Collier, M. de Angelis, D. Hammond, J. McManus, G. Rehder, and A. Tréhu (1998), Geochemical observations on Hydrate Ridge, Cascadia Margin during R/V BROWN-ROPOS cruise, August, 1998, *COAS Data Rep. 171*, 47 pp., Oregon State Univ., Corvallis.
Torres, M. E., G. Bohrmann, K. Brown, M. de Angelis, D. Hammond, G. Klinkhammer, J. McManus, E. Suess, and A. Tréhu (1999), Geochemical observations on Hydrate Ridge, Cascadia margin during R/V *Atlantis* cruise AT 3-35b, July 1999, *COAS Data Rep. 174*, Oregon State Univ., Corvallis.
Torres, M. E., J. McManus, M. D. Tryon, K. M. Brown, D. Hammond, S. Colbert, E. Suess, and K. Heeschen (2002), Fluid and chemical fluxes in and out of sediments hosting methane hydrate deposits on Hydrate Ridge, OR: I. Hydrological provinces, *Earth Planet. Sci Lett.*, *201*, 525–540.
Tréhu, A. M., and E. R. Flueh (2001), Estimating the thickness of the free gas zone beneath Hydrate Ridge, Oregon continental margin, from seismic velocities and attenuation, *J. Geophys. Res.*, *106*(B2), 2035–2045.
Tréhu, A. M., G. Lin, E. Maxwell, and C. Goldfinger (1995), A seismic reflection profile across the Cascadia subduction zone offshore central Oregon: New constraints on methane distribution and crustal structure, *J. Geophys. Res.*, *100*(B8), 15,101–15,116.
Tréhu, A. M., M. E. Torres, G. F. Moore, E. Suess, and G. Bohrmann (1999), Temporal and spatial evolution of a gas hydrate–bearing ridge on the Oregon continental margin, *Geology*, *27*, 939–942.
Tréhu, A. M., et al. (2004), Three-dimensional distribution of gas hydrate beneath southern Hydrate Ridge: Constraints from ODP Leg 204, *Earth Planet. Sci. Lett.*, *222*, 845–862.
Tryon, M. D., K. M. Brown, M. E. Torres, A. M. Tréhu, J. McManus, and R. W. Collier (1999), Measurements of transient and downward fluid flow near episodic methane gas vents, Hydrate Ridge, Cascadia, *Geology*, *27*, 1075–1078.
Tryon, M. D., K. M. Brown, and M. E. Torres (2002), Fluid and chemical flux in and out of sediments hosting methane hydrate deposits on Hydrate Ridge, OR: II. Hydrological processes, *Earth Planet. Sci. Lett.*, *222*, 541–557.
Valentine, D. L., D. C. Blanton, W. S. Reeburgh, and M. Kastner (2001), Water column methane oxidation adjacent to an area of active hydrate dissolution, Eel River Basin, *Geochim. Cosmochim. Acta*, *65*(16), 2633–2640.
Ward, B. B., and K. A. Kilpatrick (1993), Methane oxidation associated with mid-depth methane maxima in the Southern California Bight, *Cont. Shelf Res.*, *13*(10), 1111–1122.
Washburn, L., M. S. Swenson, J. L. Largier, P. M. Kosro, and S. R. Ramp (1993), Cross-shelf sediment transport by an anticyclonic eddy off northern California, *Science*, *261*, 1560–1564.
Weiss, R. F. (1970), The solubility of nitrogen, oxygen and argon in water and seawater, *Deep Sea Res.*, *17*, 721–735.
Westbrook, G. K., B. Carson, and S. S. Party (1994), Summary of Cascadia drilling results, *Proc. Ocean Drill. Program Initial Rep.*, *146*(1), 389–396.
Whiticar, M. (1999), Carbon and hydrogen isotope systematics of bacterial formation and oxidation of methane, *Chem. Geol.*, *161*, 291–314.
Wiesenburg, D. A., and N. L. Guinasso Jr. (1979), Equilibrium solubilities of methane, carbon monoxide, and hydrogen in water in sea water, *J. Chem. Eng. Data*, *24*(4), 356–360.

R. W. Collier and G. P. Klinkhammer, College of Oceanographic and Atmospheric Sciences (COAS), Oregon State University, Ocean Administration Building 104, Corvallis, OR 97331-5503, USA.
M. A. de Angelis, Oceanography Department, Humboldt State University, 1 Harpst Street, Arcata, CA 95521-8299, USA.
K. U. Heeschen, RCOM, University of Bremen, P.O. Box 330 440, D-28334 Bremen, Germany. (heeschen@uni-bremen.de)
P. Linke, G. Rehder, and E. Suess, GEOMAR Research Center for Marine Geology, Wischhofstrasse 1-3, D-24148 Kiel, Germany.

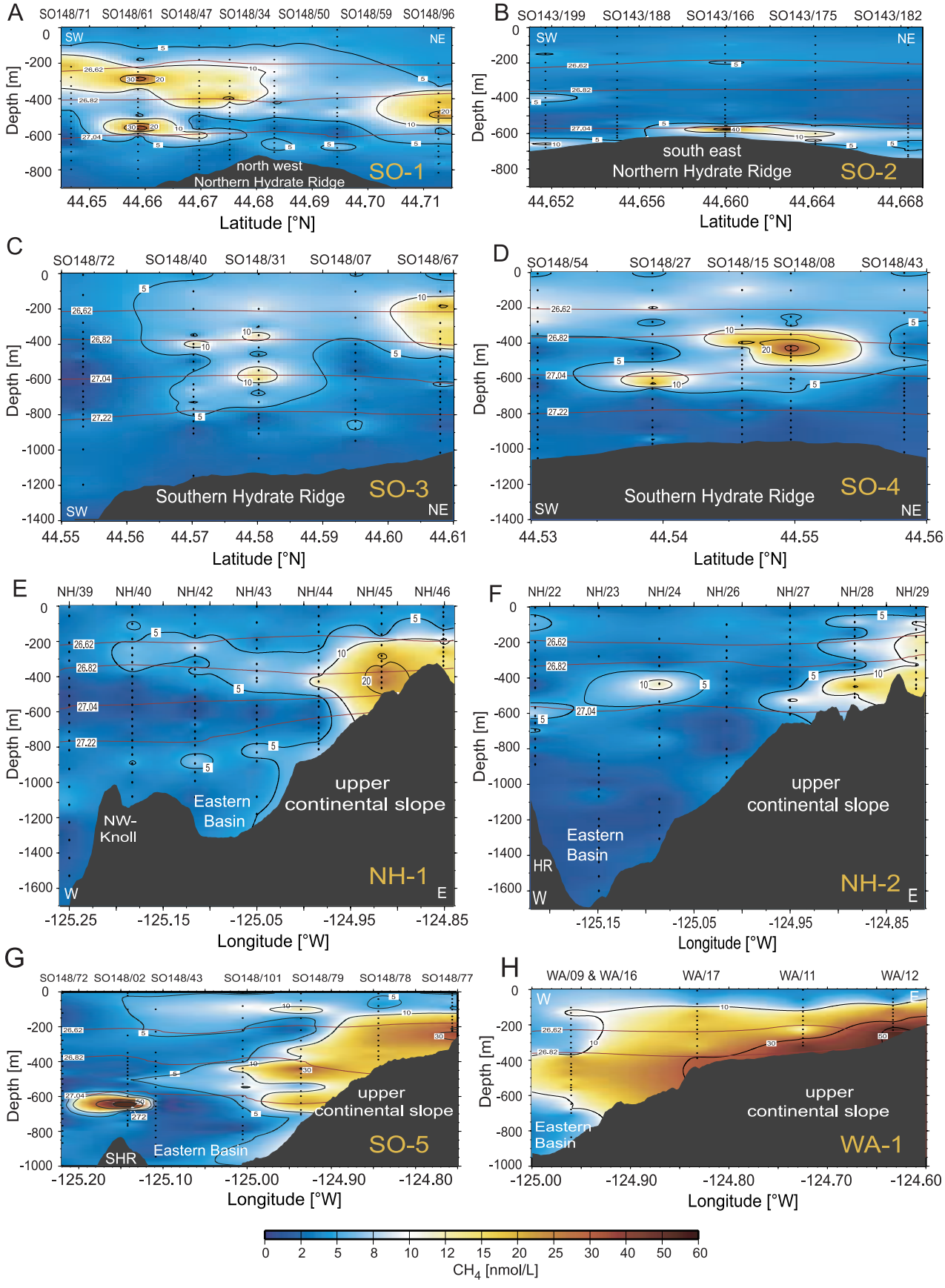
A
SO148/71 SO148/61 SO148/47 SO148/34 SO148/50 SO148/59 SO148/96
SW
NE
north west
Northern Hydrate Ridge
SO-1
Depth [m]
Latitude [°N]
B
SO143/199 SO143/188 SO143/166 SO143/175 SO143/182
SW
NE
south east
Northern Hydrate Ridge
SO-2
Depth [m]
Latitude [°N]
C
SO148/72 SO148/40 SO148/31 SO148/07 SO148/67
Southern Hydrate Ridge
SO-3
SW
NE
Depth [m]
Latitude [°N]
D
SO148/54 SO148/27 SO148/15 SO148/08 SO148/43
Southern Hydrate Ridge
SO-4
SW
NE
Depth [m]
Latitude [°N]
E
NH/39 NH/40 NH/42 NH/43 NH/44 NH/45 NH/46
NW-
Knoll
Eastern
Basin
upper
continental slope
NH-1
W
E
Depth [m]
Longitude [°W]
F
NH/22 NH/23 NH/24 NH/26 NH/27 NH/28 NH/29
Eastern
Basin
upper
continental slope
HR
NH-2
W
E
Depth [m]
Longitude [°W]
G
SO148/72 SO148/02 SO148/43 SO148/101 SO148/79 SO148/78 SO148/77
upper
continental slope
SHR
Eastern Basin
SO-5
Depth [m]
Longitude [°W]
H
WA/09 & WA/16 WA/17 WA/11 WA/12
W
E
upper
continental slope
Eastern
Basin
WA-1
Depth [m]
Longitude [°W]
0 2 5 8 10 12 15 20 25 30 40 50 60
CH4 [nmol/L]

Figure 5

Figure 5. Methane concentrations along regional transects shown in Figure 1. (a, b) SO-1 and SO-2, showing cross sections from NE-SW transects in the area of NHR; (c, d) SO-3 and SO-4, showing cross sections from NE-SW near SHR. (e, f, g) NH-1, NH-2, and SO-5, showing cross sections from the upper continental slope to the HR areas; (h) WA-1, showing a cross section of the upper slope only. Note that there is considerable variation in the latitudinal and longitudinal scales of the figures. The black dots indicate all samples taken, and station numbers are annotated in the top of each figure. The density distribution is shown by the annotated white (red) contours.